UNIVERSITY OF CALIFORNIA
RIVERSIDE

Constraining Self-Interacting Dark Matter With Astrophysical Systems

A Dissertation submitted in partial satisfaction
of the requirements for the degree of

Doctor of Philosophy

in

Physics

by

Gerardo Alvarez Jr

December 2021

Dissertation Committee:
Dr. Hai-Bo Yu, Chairperson
Dr. Yanou Cui
Dr. Philip Tanedo

The Dissertation of Gerardo Alvarez Jr is approved:

Committee Chairperson

University of California, Riverside

ACKNOWLEDGEMENTS

I would like to state my admiration and appreciation to my advisor Dr. Hai-Bo Yu for his support and direction throughout my time as a PhD candidate. It was through his guidance that the completion of this thesis and work contained therein was made possible. I also have a deep respect for the other members of this committee, Dr. Yanou Cui and Dr. Phillip Tanedo, and am grateful for many instrumental discussions with them about physics.

Dr. Aniket Joglekar has been a great help and role model throughout my experience as a graduate student. I give thanks to him and also give thanks to all the physics graduate students, notably Micheal Shamma, Ian Chaffey, Wei-Xiang Feng, Lexi Constantino, Adam Green, and Mehrdad Phoroutan for many illuminating conversations about physics and camaraderie throughout my candidacy.

I have immense love for my wife and daughter whom are my inspiration. I would also like to express love to my mom, dad and two brothers. A special thanks to Ronald Melendrez and Josue Rodriguez for many long nights of coffee and fast food fueled study sessions. Thank you to Rodolfo Rodriguez for the Peskin and Schroeder text book that I am still indebted for. Finally, I would like to thank Kenny and Lerby Sanchez for weekly jam sessions that were instrumental in retaining my sanity.

I dedicate this work to my wife Jocelyn and daughter Selma

ABSTRACT OF THE DISSERTATION

Constraining Self-Interacting Dark Matter With Astrophysical Systems

by

Gerardo Alvarez Jr

Doctor of Philosophy, Graduate Program in Physics
University of California, Riverside, December 2021
Dr. Hai-Bo Yu, Chairperson

With all of the success of the Standard Model (SM) of particle physics there are still looming inconsistencies between the model and observations. The open questions in high energy physics motivate models of physics beyond the SM. Of the natural phenomena still not explained by the SM, perhaps the biggest open question is the nature of dark matter. To date, there have been no conclusive direct detection signals of dark matter and what we know about the mysterious substance remains relegated to gravitational effects dark matter has on ordinary matter.

This work is focused on studying the constraints that astrophysical systems can place on models of dark matter. In particular, this work studies models of dark matter that exhibit self-interactions. It is shown here how inelastic models of dark matter which self-interact through the exchange of a light mediator can have observational effects on halo dynamics.

Self-interactions can play an important role in annihilation signals in the central regions of halos when a black hole is present. It has been previously shown that the constraints from annihilation signals rule out much of the WIMP parameter space. It is shown here that models of self-interacting dark matter can significantly weaken these constraints, reviving much of the parameter space. In the very dense environment of a Neutron Star (NS), scattering events between dark matter and standard model particles can impart a significant amount of thermal energy. This work shows how the inelastic model of self-interacting dark matter can be probed using NS heating. Inelastic models of dark matter have previously been shown to be able to escape direct detection signals. It is shown here that in the parameter space where direct detection is no longer sensitive to inelastic dark matter, NS heating can still probe the model. In other parts of the parameter space, NS heating is superior to or complementary to terrestrial direct detection experiments. Given the absence of terrestrial direct detection signals, looking towards astrophysical systems as particle detectors is a very interesting and exciting avenue to probe the nature of dark matter.

TABLE OF CONTENTS

LIST OF TABLES

LIST OF FIGURES

CHAPTER 1

INTRODUCTION

1.1 Standard Model

The Standard Model (SM) of particle physics groups together all known fundamental particles and their interactions. In this framework, matter particles are grouped into fermions which interact through the exchange of force carrying bosons. For each of the fundamental forces, with the exception of gravity which is not contained within the framework of the SM, there are corresponding bosonic mediators. In addition, the SM contains the Higgs Boson which is responsible for the fundamental particles receiving their mass through the spontaneous symmetry breaking mechanism [1, 2]. Mathematically, the SM can be understood as the group $\mathrm{SU_C}(3) \times \mathrm{SU_L}(2) \times \mathrm{U_Y}(1)$ [3, 4, 5, 6, 7, 8]. Particles charged under the $\mathrm{SU_C}(3)$ group carry color charge and interact via the exchange of gluons, the carriers of the strong nuclear force. The group $\mathrm{SU_L}(2) \times \mathrm{U_Y}(1)$ is spontaneously broken when the Higgs field receives a vacuum expectation value at energies below the electroweak scale to produce the group $\mathrm{U_{EM}}(1)$. Three of the massless bosons charged under $\mathrm{SU_L}(2) \times \mathrm{U_Y}(1)$ electroweak group receive a mass after spontaneous symmetry breaking while the fourth boson remains massless under the $\mathrm{U_{EM}}(1)$ electromagnetic group. The bosons that receive mass are the charged W bosons and the neutral Z boson, the carriers of the weak nuclear force. The remaining massless boson is the photon, the carrier of the electromagnetic force.

The matter particles of the SM are subdivided into leptons and quarks. Leptons consist of electron type and neutrino type particles while the quarks come in Up type and Down type particles. Both the leptons and the quarks come in three generations which become successively more massive. At least three generations of fermions are required in order to

	Particle Content	Q	Y	T_3
Leptons	$\mathrm{e_L}, \mu_\mathrm{L}, \tau_\mathrm{L}$	-1	-1	-1/2
	$\nu_\mathrm{e}, \nu_\mu, \nu_\tau$	0	-1	+1/2
	$\mathrm{e_R}, \mu_\mathrm{R}, \tau_\mathrm{R}$	-1	-2	0
Quarks	$\mathrm{u_L}, \mathrm{c_L}, \mathrm{t_L}$	+2/3	+1/3	+1/2
	$\mathrm{d_L}, \mathrm{s_L}, \mathrm{b_L}$	-1/3	+1/3	-1/2
	$\mathrm{u_R}, \mathrm{c_R}, \mathrm{t_R}$	+2/3	+4/3	0
	$\mathrm{d_R}, \mathrm{s_R}, \mathrm{b_R}$	-1/3	-2/3	0
EM	γ	0	0	0
Weak	$\mathrm{W}^\pm$	± 1	0	± 1
	Z	0	0	0
Strong	g	0	0	0
Higgs	h	0	+1	-1/2

Table 1.1: Particle content of the Standard Model with corresponding charge assignments.

explain the experimentally observed CP violation in the weak interactions [9, 10]. For three generations of matter particles a complex phase is introduced in the mass eigenstate mixing matrices called the CKM matrices. This complex phase is responsible for the observed CP violation. The quarks are charged under the $\mathrm{SU_C}(3)$ color group and exhibit a property called asymptotic freedom which requires that only colorless bound states of quarks can exist at the universe's current energy scale [11, 12]. For this reason, quarks must come in either particle - antiparticle pairs called mesons or in colorless triplets called baryons. The quarks as well as the electron type leptons receive a mass after spontaneous symmetry breaking. However, in the SM the neutrinos remain massless. Table 1.1 summarizes the particle content and the corresponding quantum numbers of the SM.

The non-Abelian gauge theory that comprises the SM has been a very successful physical model of the particle content of the universe. The SM predicted particles such as the W and Z vector bosons, the gluons, the top and charm quarks and the Higgs scalar boson before they were observed experimentally [13, 14, 15, 16, 17]. There are also various high precision measurements which agree with the SM to unprecedented accuracy [18, 19].

However, there are discrepancies that exist between the SM and observation. For instance, there is overwhelming evidence that the neutrinos have a small non zero mass whereas the SM predicts that neutrinos are exactly massless [20, 21, 22]. There is the open question about strong CP violation. There is an allowed operator in the $\mathrm{SU_C}(3)$ portion of the SM lagrangian which would violate CP symmetry. However, experimentally this term is not observed in nature [23, 24]. The SM also predicts that matter and antimatter should be created in roughly equal quantities in the early universe. What is observed is that the universe is formed predominantly and overwhelmingly out of matter. The baryon asymmetry problem seeks to answer the question of the missing antimatter [25, 26, 27]. Perhaps the most mysterious of the open questions related to the SM is the nature of dark energy of which very little is known. Dark energy is the name given to the substance responsible for the observed accelerated expansion of the universe. Dark energy is typically modeled as a constant energy density throughout the cosmos which acts with negative pressure on the curvature of spacetime and dominates the universe's energy budget [28, 29]. These are but a few of the open questions related to the SM of particle physics which motivates physics beyond the SM. The open question that this work is focused on is the dark matter problem. There are various observations that show there is a mysterious substance throughout the cosmos called dark matter that takes up a large portion of the universe's matter-energy budget and does not fit within the framework of the SM. This work takes a phenomenological approach to the dark matter problem and shows how astrophysical observations can put constraints on dark matter models.

1.2 Dark Matter

Estimates of the gravitational mass of the Coma Cluster show that there is significantly more mass in the cluster than what is observed when compared to the luminous mass of

the cluster [30, 31]. This observation is one of the first pieces of evidence of dark matter. Galactic velocity rotational curves show that galaxies are spinning too fast for the amount of luminous mass that is observed [32, 33]. If the galaxies only contain the mass that is seen then the rotational velocity of the stellar distribution should drop off at large radii. What is observed is that stars outside the bulk of the galactic disk have a velocity that is roughly a constant with increasing radius, as shown in Fig. 1.1. This implies that there is some unseen mass distributed at very large radii compared to the size of the galactic disk which creates a gravitational well holding the galaxy together. Furthermore, x-ray and gravitational lensing observations of the Bullet Cluster show two clusters which have collided and the luminous matter has been separated from the gravitational matter. This shows that dark matter does not interact strongly with the SM and it also puts constraints on the strength of possible dark matter self-interactions [34, 35]. Studying the anisotropy of the cosmic microwave background, the relative quantities of the different types of matter and energy in the universe can be understood [36, 37]. Fig. 1.2 shows the theoretical fit to the observed cosmic microwave background anisotropy. Changing the relative quantities of dark matter, dark energy and the baryonic component will change the locations and amplitudes of the peaks found in Fig. 1.2. Current measurements show that the universe is composed of $\sim \%69$ dark energy, $\sim 26\%$ dark matter, and only about $\sim 5\%$ baryonic matter including radiation.

It is now understood that the majority of galaxies are housed inside of a dark matter halo and that dark matter plays a crucial role in structure formation in the universe [38, 39]. However, little is known about the nature of dark matter. There is a large playground for theoretical physicists to play around in when creating models for dark matter. It is hypothesized that dark matter may be primordial black holes or a form of dark baryonic matter called Massive Compact Objects also known as MACHO's [40]. It has been shown that these models of dark matter can only account for a small fraction of the cosmic relic

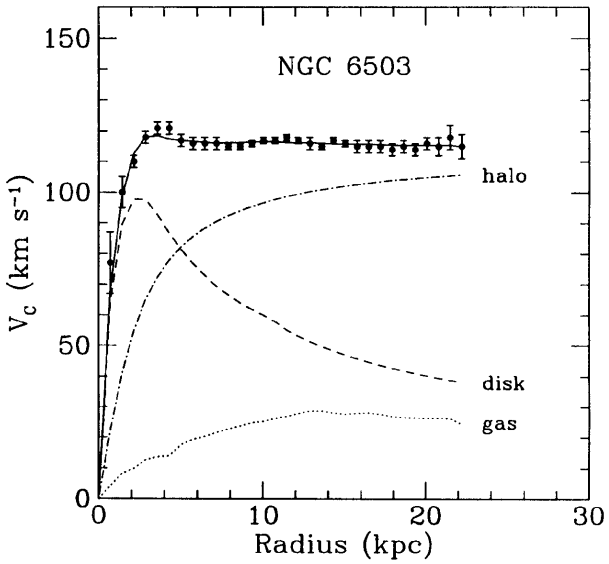

Figure 1.1: Galactic velocity rotation curve for NGC 6503 taken from [36]. Solid black shows the best fit line to observed data points. Dashed black shows the expected velocity curve for the central disk without the dark matter halo component (dashed dotted).

abundance of dark matter, about $\sim 20\%$. The conservative approach to dark matter, and the approach taken in this work, is to assume that it is some type of fundamental particle. The observations surrounding dark matter point to a cosmologically stable and electrically neutral fundamental particle [41, 42, 43]. Any model of dark matter must also reproduce the observed cosmic relic abundance of dark matter. The relic abundance of dark matter is typically reported as $h^2\Omega_{\rm DM} \sim 0.11933$ where $\Omega_{\rm DM}$ is the dark matter energy density normalized to the critical density and h is the reduced Hubble constant [44, 45]. The only SM particle which is cosmologically stable and electrically neutral is the neutrino. However, it has been shown that if the neutrino were to reproduce the relic abundance of dark matter it would also disrupt structure formation due to its relativistic nature [46, 47, 48]. Therefore, dark matter must also be cold in order to reproduce the CMB power spectrum. There is no such particle in the SM that fits all of these criteria and physics beyond the SM is required to understand dark matter.

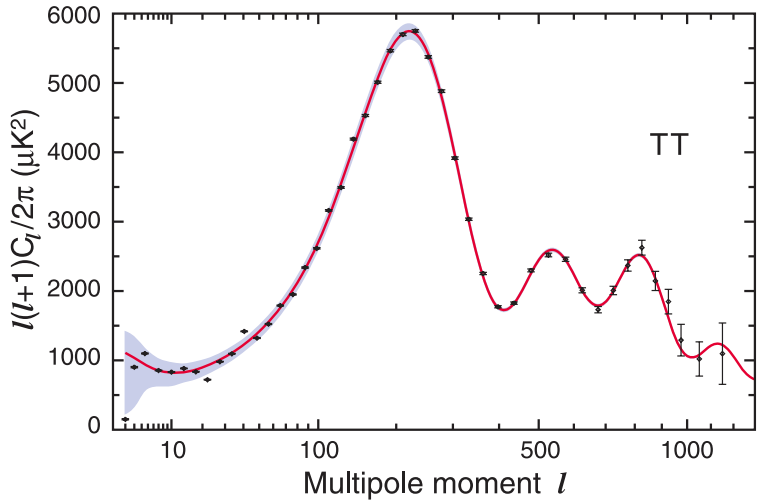

Figure 1.2: Cosmic microwave background anisotropy plot taken from [37]. The red curve shows the theoretical fit to the observed data points in black.

The generally accepted model for dark matter is the ΛCDM paradigm which has been able to reproduce many of the cosmological observations. The paradigm has two essential ingredients, a cosmological constant Λ playing the role of dark energy and a new non-relativistic, collision-less and massive fundamental particle playing the role of dark matter. Within this paradigm, a highly studied model of dark matter is the WIMP model. The WIMP model has a dark matter particle with a mass and annihilation cross section on the weak scale. Within this model it is assumed that dark matter is produced thermally in the early universe in the freeze out scenario. With the assumption of a thermal production along with a mass and cross section at the weak scale, the model naturally reproduces the observed relic abundance of dark matter. This coincidence is often referred to as the WIMP miracle. However successful the model, there are growing tensions between the model and observations at galactic scales. There are also tight constraints on the model from direct detection and collider experiments.

1.3 Self-Interacting Dark Matter

The ΛCDM model reproduces large scale observations very well but there are so called small scale structure problems with the model. Simulations of collisionless dark matter predict that there should be more satellite galaxies orbiting galaxies like the Milky Way than are observed. This is referred to as the missing satellite problem. It has been suggested that this is because the smaller galaxies have smaller stellar production so that they are very difficult to observe. However, simulations show that the satellite galaxies should have enough mass to have a significant amount of stellar production. This gives rise to the too big to fail problem of dark matter sub-halos; the subhalos are too big to fail at producing stars. An even greater tension between the ΛCDM model and observation is the core vs. cusp problem. Observations show that many dwarf galaxies prefer to have a cored density profile in the central regions of their halo while the collisionless dark matter model predicts a steeper cusp. However, not all small scale dwarf and LSB galaxies prefer a cored profile and there is a diversity of profiles ranging from cored to cuspy profiles. Explaining the range of observed density profiles is referred to as the diversity problem. For a review on the small scale structure issues see [49, 50, 51].

To alleviate the tensions between small scale structure observations and dark matter models it has been proposed that dark matter may exhibit self-interactions in a model called Self-Interacting Dark Matter (SIDM) [52, 53]. In the central regions of dark matter halos where the density is greater, the self-interaction rate can be large enough to thermalize the halo. Thermal energy is transported from the inner regions of the halo to the outer regions causing the halo to puff up producing a core, thus explaining the core vs. cusp problem. The self-scattering cross section required to explain the cored profiles is $\sigma/m_\chi \sim 1\ \mathrm{cm}^2/\mathrm{g}$ on the dwarf galaxy scale, where m_χ is the dark matter mass. Fig. 1.3 (left) shows how self-interactions give rise to a cored profile compared to the cuspy profile produced by

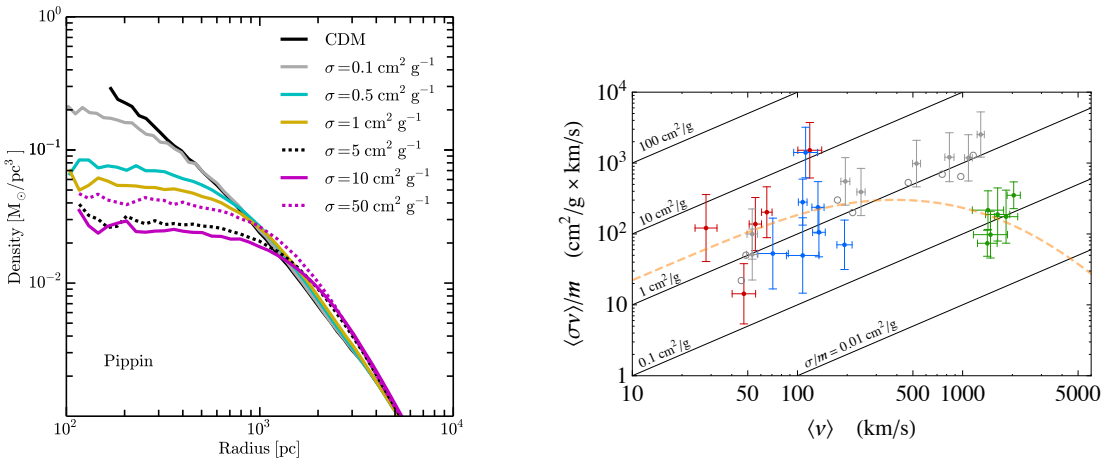

Figure 1.3: Left: Dark matter central density profiles in the self-interacting dark matter model for various scattering cross sections compared the collisionless dark matter model (black). Right: Self-scattering cross section as a function of velocity (dashed) and observational bounds for dwarf galaxies (red), LSB galaxies (blue), and clusters (green). Gray data is mock data from numerical simulations. Plots taken from reference [53].

collisionless dark matter. Furthermore, if a dark matter halo contains a significant amount of baryonic matter then the gravitational effects of the baryonic component must be taken under consideration. When including the baryonic component, the gravitational well in the central regions of the halo become steeper driving dark matter back into a cusp profile. Depending on how significant the baryonic component is in the halo, a range of density profiles from a cored profile to a cusp profile can be produced. This is the origin of the diversity problem [54, 55]. Simulations of SIDM also predict that fewer satellite galaxies are formed explaining the missing satellite and too big to fail problems [56, 57].

There are also observational consequences for SIDM on the scale of galaxy clusters. For instance, if the self-scattering is too large then the model is in tension with the bullet cluster observation [34, 35]. Strong self-scattering would prevent the dark matter from separating from the baryonic matter as observed in the collision of the two clusters in the bullet cluster. Therefore, the self-scattering cross section is required to be less than $\sigma/m_\chi \sim 0.1\ \mathrm{cm}^2/\mathrm{g}$ at

the cluster scale. The various requirements for the normalized self-scattering cross section at different scales requires a velocity dependent self-scattering. Models of SIDM naturally predict a self-scattering cross section which is velocity dependent and typically decreases with velocity [58]. It has been shown that SIDM can achieve the correct self-scattering cross section at the various scales and simultaneously predict the correct relic abundance through the freeze out scenario [53]. Fig. 1.3 (right) shows the self-scattering cross section at various scales and the corresponding bounds. The SIDM model inherits all of the large-scale cosmological success of the collisionless counterpart but also can further explain the small scale structure problems present in the collisionless paradigm.

This work proposes novel astrophysical probes to constrain the SIDM model framework. This work is largely based on the following publications by this author and company [59, 60, 61]. First, a model of inelastic self-interacting dark matter and its halo dynamic constraints are studied in Chapter 2. In Chapter 3, annihilation signals from SIDM density spikes near black holes and their indirect detection constraints are presented. The sensitivity from the heating of neutron stars from inelastic SIDM with relativistic targets is shown in Chapter 4. Finally, a discussion and concluding remarks are found in Chapter 5.

CHAPTER 2

ASTROPHYSICAL PROBES OF INELASTIC SELF-INTERACTING DARK MATTER

Many SIDM models assume there is only one dark matter state and a light force carrier mediates elastic dark matter self-scattering in the halo, see, e.g., [53]. In this case, the initial and final states in the collisions are the same, and they only redistribute energy of dark matter particles as the halo as a whole does not lose energy. More recently, there is growing interest in considering particle physics realizations of SIDM with multiple states. For example, to avoid strong bounds from direct detection experiments [62, 63, 64, 65, 66], Refs. [67, 68] propose an inelastic SIDM model, where there are two dark states and they differ by a small mass splitting [69, 70]. One can adjust the splitting to kinematically forbid transitional up-scattering in nuclear recoils, but still allow strong elastic self-interactions between two light states in the halo. In addition, Ref. [71] studies dark matter self-interactions in the exciting dark matter model [72, 73, 74, 75], where dark matter collisions can produce a heavy state that subsequently decays back to the light one and a standard model particle. More generally, if the SIDM candidate is made of composite states, such as dark atoms [76, 77, 78, 79, 80, 81, 82, 83, 84, 85, 86] and strongly-coupled particles [87, 88, 89, 90], it is natural to expect inelastic excitations during dark matter collisions in dark halos.

In this chapter, we consider an inelastic SIDM model and study its astrophysical implications. It assumes that a Majorana mass term induces a small mass splitting between two fermionic dark matter states and they interact with a U(1) gauge boson. We assume the gauge boson is light and develop a numerical method to calculate both elastic

and inelastic dark matter self-scattering cross sections. After imposing the relic abundance constraint on the gauge coupling constant, we focus on benchmark dark matter masses, which cover a wide range from $10\ \mathrm{MeV}$ to $160\ \mathrm{GeV}$, and search for parameter regions where the elastic self-scattering cross section per unit mass (σ_V/m_χ) satisfies $1\ \mathrm{cm}^2/\mathrm{g} \leq \sigma_V/m_\chi \leq 5\ \mathrm{cm}^2/\mathrm{g}$, as favored by observations on galactic scales [53]. Our work is a natural and simple extension to the minimal SIDM model that contains only one dark matter state, but calculations of the self-scattering cross sections in the current model are much more challenging than the minimal one [91, 58]. In addition, we explore a broader mass range for both dark matter and mediator particles, compared to earlier studies [68]. As we will show, for the dark matter mass below $\sim 1\ \mathrm{GeV}$, inelastic up scattering dominates over elastic one if the former is kinematically open in the dark halo. This has important implications for constraining the parameter space.

We further consider the endothermic up-scattering process of dark matter particles and its influence on halo evolution and inner halo structure. If the heavy state decays back to the light state by releasing a massless species, the SIDM halo profile can become cuspy again, because the dissipative self-interactions can cool the inner halo [92] and speed up the onset of core collapse [93, 94]. Using dwarf galaxies that show density cores, Ref. [93] derives constraints on parameters that characterize the cooling rate of dissipative dark matter collisions. In this work, we will take the results in [93] to further narrow down parameter space of the inelastic SIDM model.

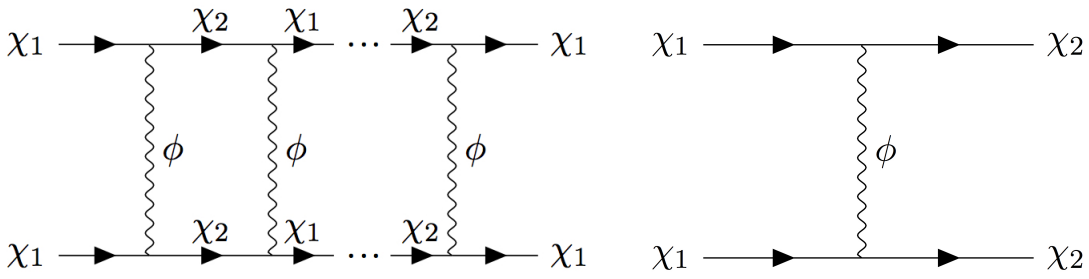

Figure 2.1: Feynman diagrams for elastic (left) and inelastic (right) dark matter self-interactions.

2.1 Particle Physics Model for iSIDM

We assume that the dark matter particle is a fermion (Ψ) and it interacts with a dark U(1) gauge boson (ϕ_μ). The model can be described by the following Lagrangian [72, 73, 71]

$$\mathcal{L} = \bar{\Psi}(i\partial\!\!\!/ - m)\Psi - \frac{\delta m}{4}(\bar{\Psi}\Psi^c + \bar{\Psi}^c\Psi) + -\frac{1}{4}\phi^{\mu\nu}\phi_{\mu\nu} + \frac{1}{2}m_\phi^2\phi^\mu\phi_\mu + g_\chi\bar{\Psi}\gamma^\mu\Psi\phi_\mu \quad (2.1)$$

where Ψ^c is the charge conjugation of Ψ, $\phi_{\mu\nu}$ is the field strength of ϕ_ν, g_χ is the gauge coupling constant, m is the Dirac mass of the dark matter state and δm is its Majorana mass. In this work, we assume $m \gg \delta m$. Defining the Majorana mass eigenstates as $\chi_1 = i(\Psi - \Psi^c)/\sqrt{2}$ and $\chi_2 = (\Psi + \Psi^c)/\sqrt{2}$, we rewrite equation (2.1) as

$$\mathcal{L} \supset \frac{1}{2}\bar{\chi}_1\left(i\partial\!\!\!/ - m_\chi\right)\chi_1 + \frac{1}{2}\bar{\chi}_2\left(i\partial\!\!\!/ - (m_\chi + \delta m)\right)\chi_2 + \frac{i}{2}g_\chi\bar{\chi}_2\gamma^\mu\chi_1\phi_\mu + \text{h.c.} \quad (2.2)$$

where $m_\chi = m - \delta m/2$ is the mass of the light state χ_1.

Since the mass eigenstates are Majorana states, they carry no charge and only interact through an off-diagonal coupling. The relevant Feynman diagrams for both elastic and inelastic dark matter self-scattering are shown in Fig. 2.1. The tree-level elastic scattering process involves mixed initial and final states. All other elastic scatterings occur through

high-order box or ladder diagrams. As the universe cools, the up-scattering process becomes kinematically unfavorable, driving the density of the heavy state down [68, 95]. Thus, we assume dark matter is made of the light state in the halo and only consider elastic and inelastic scattering processes shown in the left and right panels of Fig. 2.1, respectively.

In the non-relativistic limit, we can apply the Schrödinger formalism. There are two wave functions coupled by a matrix potential of the form

$$i\frac{\partial}{\partial t}\tilde{\psi} = \left[-\frac{1}{2\mu}\nabla^2 + \mathbf{V}\right]\tilde{\psi} \tag{2.3}$$

where $\mu = m_\chi/2$ is the reduced mass, the vector $\tilde{\psi}^T = \left[\psi_1\ ,\ \psi_2\right]$ detonate the wave functions for the two particle modes, and the matrix potential $\mathbf{V}$ is

$$\mathbf{V} = \begin{bmatrix} 0 & -\frac{\alpha_\chi}{r}e^{-m_\phi r} \\ -\frac{\alpha_\chi}{r}e^{-m_\phi r} & 2\delta m \end{bmatrix}. \tag{2.4}$$

We have defined $\alpha_\chi \equiv g_\chi^2/4\pi$ as the dark fine structure constant. The energy needed to create the heavy state as a pair is $2\delta m$. The numerical solution to this set of coupled differential equations gives the scattering cross sections through the method of partial waves.

2.2 Numerical Results

We assume that dark matter freezes out in the early universe with the relic abundance to be consistent with the observed density. In this paper, we set the dark fine structure constant to $\alpha_\chi = 0.01\,(m_\chi/270\ \mathrm{GeV})$ such that the annihilation cross section is $6\times10^{-26}\ \mathrm{cm}^2/\mathrm{g}$. The dark matter self-scattering cross sections, both elastic and inelastic, are in general velocity-dependent. To capture the relevant physics on dwarf scales, we set the dark matter relative velocity to be $60\ \mathrm{km/s}$ in the halo throughout this paper unless otherwise stated. The model

is left with three free parameters, the dark matter mass m_χ, the mass splitting δm and the mediator mass m_ϕ.

Performing separation of variables on equation (2.3), we have the radial equation

$$\left[\frac{1}{r^2}\frac{\partial}{\partial r}\left(r^2\frac{\partial}{\partial r}\right) - \frac{l(l+1)}{r^2} + k^2\right] R_{l,i}(r) = m_\chi V_{i,j} R_{l,j}(r) \tag{2.5}$$

where l is the angular momentum mode, k is the magnitude of the wave vector, $R_{l,i}(r)$ are the radial wave functions for $i = 1, 2$ and $V_{i,j}$ denotes components of the matrix (2.4). Defining the following dimensionless parameters and substitutions,

$$x \equiv 2\alpha_\chi \mu r, \;\; a \equiv \frac{v}{2\alpha_\chi}, \;\; b \equiv \frac{2\alpha_\chi \mu}{m_\phi}, \;\; c^2 \equiv a^2 - \frac{\delta m}{\mu \alpha_\chi^2}, \;\; \chi_{l,i}(x) \equiv x R_{l,i}(x) \tag{2.6}$$

we rewrite the radial equation (2.5) in the matrix form as

$$\frac{d^2}{dx^2}\begin{bmatrix}\chi_{l,1}\\ \chi_{l,2}\end{bmatrix} = \begin{bmatrix}\frac{l(l+1)}{x^2} - a^2 & -\frac{1}{x}e^{-\frac{x}{b}}\\ -\frac{1}{x}e^{-\frac{x}{b}} & \frac{l(l+1)}{x^2} - c^2\end{bmatrix}\begin{bmatrix}\chi_{l,1}\\ \chi_{l,2}\end{bmatrix}. \tag{2.7}$$

The wave function can be expanded in terms of spherical waves,

$$\tilde{\psi} = \sum_{l=0}^{\infty}(2l+1)P_l(\cos\theta)\left[\tilde{\psi}_{\rm in}\frac{e^{ip_{\rm in}x} - (-1)^l e^{-ip_{\rm in}x}}{2ip_{\rm in}x} + \begin{pmatrix}\alpha_\chi m_\chi \mathcal{F}_{x,l}\frac{e^{iax}}{x}\\ \alpha_\chi m_\chi \mathcal{F}_{y,l}\frac{e^{icx}}{x}\end{pmatrix}\right], \tag{2.8}$$

where $\mathcal{F}_{x/y,l}$ are the scattering amplitudes for the two particle system and $p_{\rm in} = a, c$, depending on the initial state. If the initial state is χ_1 as we consider in this work, $p_{\rm in} = a$ and $\tilde{\psi}_{\rm in}^T = \begin{bmatrix}1\ ,\ 0\end{bmatrix}$. The differential cross section is given by,

$$\frac{d\sigma}{d\Omega} = \frac{p_{\rm out}}{p_{\rm in}}\left|\sum_{l=0}^{\infty}(2l+1)P_l(\cos\theta)\mathcal{F}_l\right|^2 \tag{2.9}$$

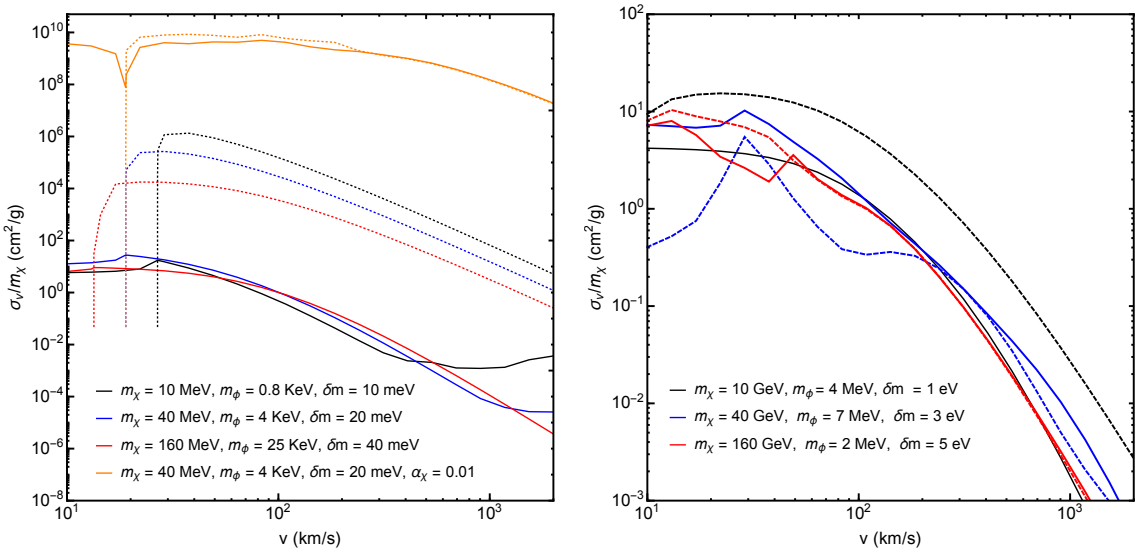

Figure 2.2: The dark matter self-scattering cross section vs the relative scattering velocity for benchmark cases with the dark matter mass in the MeV (left panel) and GeV (right panel) ranges, where we fix the dark coupling constant using the relic abundance relation, $\alpha_\chi = 0.01(m_\chi/270\ \mathrm{GeV})$. The solid and dotted curves correspond to the elastic and inelastic cross sections, respectively. For comparison, we also show a case for $m_\chi = 40\ \mathrm{MeV}$ and $\alpha_\chi = 0.01$ in the left panel.

where $p_{\rm in}$, $p_{\rm out}$ and $\mathcal{F}_l$ again depend on the initial and final states. For elastic scattering $\chi_1\chi_1 \to \chi_1\chi_1$, $p_{\rm in} = p_{\rm out} = a$ and $\mathcal{F}_l = \mathcal{F}_{x,l}$. For inelastic scattering $\chi_1\chi_1 \to \chi_2\chi_2$, $p_{\rm in} = a$, $p_{\rm out} = c$ and $\mathcal{F}_l = \mathcal{F}_{y,l}$.

To find the scattering amplitudes $\mathcal{F}_{x/y,l}$, we need to first find the wave function by numerically solving equation (2.7), and then map its form at large radii onto the spherical wave expansion in equation (2.8). However, a direct numerical solution to the wave equation (2.7) is unstable for a large part of the parameter space of interest. To tame these instabilities, we follow the procedure discussed in [96, 68] and make a number of substitutions to transform the wave equation into a more manageable form; see the appendix for details. In this work, we calculate the viscosity cross section for dark matter self-interactions [58],

$$\sigma_V = \int d\Omega \frac{d\sigma}{d\Omega} \sin^2\theta, \tag{2.10}$$

which regulates both forward and backward scatterings. See the appendix for an explicit expression of the viscosity cross section in terms of phase shifts.

In Fig. 2.2, we show the elastic (solid) and inelastic (dashed) self-scattering cross sections vs the relative velocity for a few representative cases, where we choose a wide range of dark matter masses from $10\ \mathrm{MeV}$ to $160\ \mathrm{GeV}$. Overall the cross sections decrease as the velocity increases. For dark matter masses below $1\ \mathrm{GeV}$ (left panel), there is a clear indication of the threshold velocity below which inelastic up scattering is kinematically forbidden. In this mass range, when the coupling constant is set by the relic abundance constraint [97, 98, 99, 100], i.e., $\alpha_\chi = 0.01(m_\chi/270\ \mathrm{GeV})$, the inelastic scattering cross section is much larger than the elastic one as long as the up-scattering channel is open. As we discussed, in this model, inelastic up scattering occurs at the tree-level, while elastic scattering at the high-order level. For small m_χ below $1\ \mathrm{GeV}$, the dark fine structure constant α_χ is small as well, and the non-perturbative quantum effect is absent to enhance the elastic cross section. To demonstrate this point, we present another case, where we set $\alpha_\chi = 0.01$ for $m_\chi = 40\ \mathrm{MeV}$. In this case, both elastic and inelastic cross sections are similar for the velocity larger than $18\ \mathrm{km/s}$. For high dark matter masses (right panel), the elastic and inelastic cross sections become more compatible, aside from resonance peaks, and the up-scattering process is kinematically allowed in the plotted velocity range. As m_χ increases, the gauge coupling α_χ increase accordingly and the non-perturbative effect boosts the elastic scattering cross section significantly.

2.3 Halo Dynamic Constraints

Taking the benchmark m_χ values shown in Fig. 2.2, we scan parameter space of the δm–m_ϕ plane, such that the elastic cross section fall within the range of $1\ \mathrm{cm^2/g} \leq \sigma_V/m_\chi \leq 5\ \mathrm{cm^2/g}$ for the relative velocity $60\ \mathrm{km/s}$, a characteristic value for dwarf galaxies that

prefer a dark matter density core. In Fig. 2.3, we show the resulting parameter space (shaded). For a given dark matter mass, there is a preferred range in the plane, where the elastic self-scattering cross section is large enough to thermalize the inner halo in accord with observations [53]. For all cases, if the mass splitting δm is small, the mediator mass m_ϕ is almost a constant. While, as δm increases towards the high end, m_ϕ must decrease to preserve the elastic cross section in the desired range, since the elastic process involves virtual up-scattering processes, as shown in Fig. 2.1 (left). The transition occurs when the mass splitting reaches the kinematic threshold, where up scattering is forbidden for larger values of δm, i.e., $2\delta m = \mu v_{\rm rel}^2/2$ with $v_{\rm rel} = 60$ km/s. In Fig. 2.3, the orange shaded regions are where $\chi_1\chi_1 \to \chi_2\chi_2$ is kinematically forbidden, while in the magenta and blue regions, the up scattering is allowed. Note in the case of $m_\chi = 40$ GeV there is more than one branch for the favored parameter space, because the scattering is in the strong resonance regime [101, 58] and multiple ranges of the mediator mass is allowed; see also [68].

If the mass splitting is large enough and up scattering is forbidden, dark matter self-interactions are purely elastic and the condition of $1\ {\rm cm}^2/{\rm g} \leq \sigma_V/m_\chi \leq 5\ {\rm cm}^2/{\rm g}$ is sufficient enough to specify astrophysical constraints. However, if $\chi_1\chi_1 \to \chi_2\chi_2$ is allowed in the halo and the resulting χ_2 can further decay to χ_1 and some light species, this dissipative process may cool the inner halo and speed up the SIDM core collapse [93]. For the model we consider, $m_\phi \gg \delta m$ in the parameter regions of interest, e.g., the shaded regions in Fig. 2.3, hence the decay process $\chi_2 \to \chi_1\phi$ is kinematically forbidden. On the other hand, if we consider a more general setup, there are other interaction terms that may lead to dissipative decays of χ_2. For example, Ref. [75] introduces a dimension-5 dipole operator $(1/M)\bar{\chi}_2\sigma^{\mu\nu}\chi_1 F_{\mu\nu}$, where M is the cut-off scale and $F_{\mu\nu}$ is the field strength of the standard model photon. With this operator, χ_2 can decay to χ_1 and γ. The rate is $\Gamma_{\chi_2\to\chi_1\gamma} = 4\delta m^3/(\pi M^2)$, and χ_2's lifetime is $\tau = 1/\Gamma_{\chi_2\to\chi_1\gamma} \sim 0.5\ {\rm sec}\,(M/{\rm TeV})^2\,({\rm keV}/\delta{\rm m})^3$. For

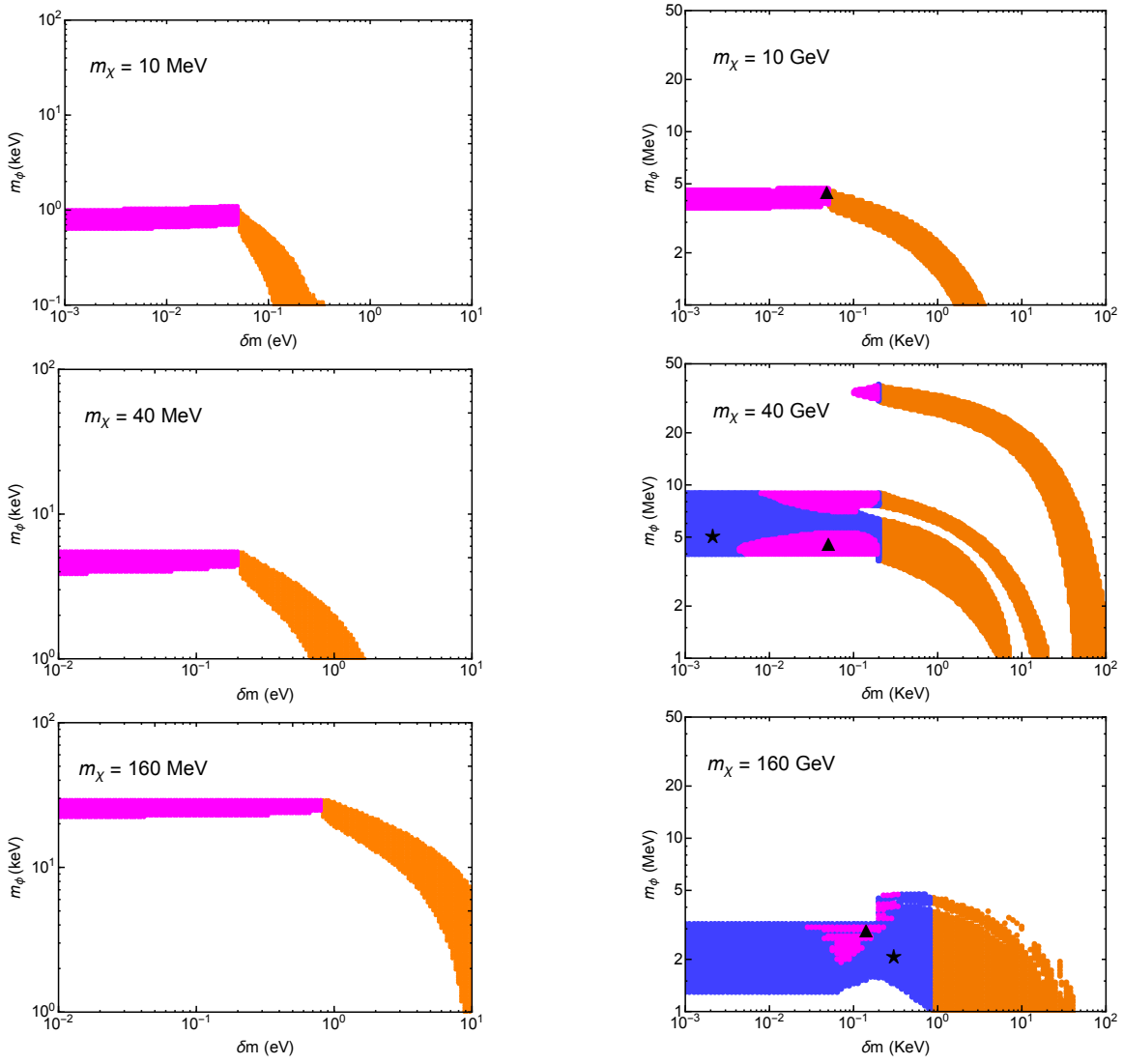

Figure 2.3: The shaded regions correspond to the accessible parameter space in the δm–m_ϕ plane, where the elastic scattering cross section is in the range of $1 \leq \sigma_V/m_\chi \leq 5\ \mathrm{cm}^2/\mathrm{g}$, favored by solving the small-scale issues. We have set the dark matter relative velocity to be $60\ \mathrm{km/s}$, a characteristic value in dwarf galaxies that prefer a dark matter density core. In the orange regions, the up-scattering process ($\chi_1\chi_1 \to \chi_2\chi_2$) is kinematically forbidden and dark matter self-interactions are purely elastic. In the magenta (blue) regions, the up-scattering process is allowed, and the dissipation process associated with the χ_2 decay can lead to core collapse in dwarf galaxies with a timescale shorter (longer) than $10\ \mathrm{Gyr}$. The starred and triangle points are references which show the mapping between the elastic scattering and the core-collapse constraints, as explicitly shown in Fig. 2.4.

$\delta m \sim 10^{-3}\mathrm{eV}$, it is comparable to the age of galaxies, $\sim 10\ \mathrm{Gyr}$, for M up to $\sim 1\ \mathrm{TeV}$. Thus, this dissipative decay is relevant to halo dynamics if the dipole operator is present. In addition, in atomic dark matter models, an excited atomic state can decay to a ground state by emitting a massless dark photon.

In what follows, we assume that χ_2 can decay to χ_1 and a massless species that escapes the halo, and study additional astrophysical constraints on the parameter space. Using dwarf galaxies that show shallow density cores, Ref. [93] derives bounds on dissipative dark matter interactions by demanding the core-collapse timescale longer than the age of galaxies, $\sim 10\ \mathrm{Gyr}$. In particular, it uses the energy loss per collision and the ratio of inelastic to elastic cross sections, i.e., $\nu_{\rm loss} = \sqrt{E_{\rm loss}/m_\chi}$ and σ'/σ, respectively, to characterize the cooling effect, and places constraints on their combinations. To apply the core-collapse constraints on our model, we set $E_{\rm loss} = \delta m$, calculate $\nu_{\rm loss}$ and σ'/σ values for each favored model point shown in Fig. 2.3 (shaded), and then compare them with the limits on the σ'/σ–$\nu_{\rm loss}$ plane from [93] as reproduced in Fig. 2.4 (gray shaded). In the magenta shaded regions of Fig. 2.3, the dissipative self-interactions are strong enough to cause core collapse in dwarf halos within $10\ \mathrm{Gyr}$. While in the blue regions, inelastic up scattering can occur, but the overall cooling rate is small to trigger core collapse in the age of galaxies.

To better understand these constraints, we show the distribution of the model points in the σ'/σ–$\nu_{\rm loss}$ plane for three benchmark cases in Fig. 2.4, along with the bounds from [93] (gray). All points (magenta) that lie within the gray regions are disfavored as they result in a core-collapse timescale too short to fit the observations; while the points (blue) outside are still allowed. We classify the model points shown in Fig. 2.3 using the same color scheme. Note we have extrapolated the disfavored parameter space following the trend beyond the upper limit of σ'/σ in [93] (black dashed). This is reasonable, because the bounds should be stronger as σ' further increases.

From Fig. 2.4, we see that as the dark matter decreases from $160\ \mathrm{GeV}$, more of the

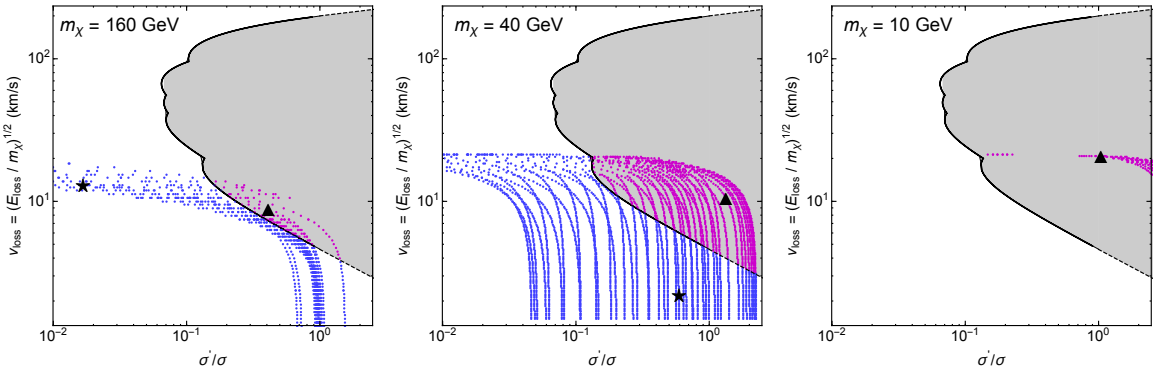

Figure 2.4: Mapping between elastic scattering and galaxy core-collapse constraints on the σ'/σ–$\nu_{\rm loss}$ plane. In the gray regions within the black contour, the halo core collapse induced by dissipative dark matter self-interactions occurs within the age of galaxies; adapted from [93]. The dashed black lines are the linear extrapolation of the contour for $\sigma'/\sigma > 1$. The magenta points that lie within the gray regions are disfavored by the core-collapse constraints; while the blue points outside are still allowed. The stars and triangles are reference points and their correspondences are shown on the δm–m_ϕ plane in Fig. 2.3.

parameter space is disfavored by the core-collapse constraints. When the mass approaches 10 GeV or smaller, the entire model points lie within the gray regions. Since the gauge coupling reduces as the dark matter mass decreases, the inelastic scattering gradually dominates over the elastic one if the former is open. For the dark matter below ~ 10 GeV, only the portion of the parameter space, where inelastic scattering is kinematically forbidden, remains viable. While for the cases of $m_\chi = 160$ GeV and 40 GeV, in some parts of the parameter space, inelastic up scattering is allowed, but the cooling rate is not significant so they evade the collapse constraints, because either the inelastic cross section or the energy loss per collision is small. We demonstrate this by using the reference points in both Figs. 2.3 and 2.4 (stars and triangles), which are in one-to-one correspondence. In the case of $m_\chi = 160$ GeV, the two references have similar δm and σ/m, but the star point has much smaller σ'/m than the triangle one as the former is closer to the threshold of the up scattering. While in the case of $m_\chi = 40$ GeV, the reference points mainly differ in δm, resulting different locations in the σ'/σ–$\nu_{\rm loss}$ plane.

2.4 Summary

This work has studied an inelastic dark matter model with a light mediator, based on a U(1) gauge symmetry. The presence of a small Majorana mass splits a Dirac fermion into two Majorana states and the light one is the dark matter candidate. In this model, both elastic and inelastic dark matter self-interactions can be present in the halo. The former is mediated by a high-order process with multiple exchanges of the light mediator; while the latter by a tree-level process when it is kinematically allowed. Using the technique of partial waves, this work has developed a numerical procedure to calculate the elastic and inelastic scattering cross sections.

Astrophysical constraints on the model parameters, i.e., the dark gauge coupling constant, dark matter mass, mediator mass and mass splitting between the two Majorana states has been explored here. First, this work imposed the relic density constraint on the coupling constant by assuming the standard freeze-out scenario, then chose six benchmark cases that cover a wide range of the dark matter mass, $10\ \mathrm{MeV}$–$160\ \mathrm{GeV}$. For each case, this work found the parameter regions, where the elastic scattering cross section falls within the range of $1\ \mathrm{cm}^2/\mathrm{g}$–$5\ \mathrm{cm}^2/\mathrm{g}$ in dwarf galaxies in order to solve the small-scale issues. This analysis shows that if the mass splitting gets too large, the kinematic suppression of the intermediate virtual processes demand that the mediator become lighter to preserve the desired elastic cross section. It was also found that when the dark matter mass decreases the inelastic scattering cross section dominates over the elastic one. This is because the coupling constant becomes smaller as the mass decreases and the non-perturbative quantum enhancement for the elastic cross section diminishes accordingly.

If the heavy state can decay to the light state and a massless degree of freedom, inelastic dark matter self-interactions may induce a dissipative process that cools the inner halo and leads to SIDM core collapse. Observations of dark matter density cores in many low

surface brightness galaxies put a constraint on the rate of energy loss. This work studied its implications for the dark matter model consider here, and found it eliminates the majority of the parameter space for dark matter masses below $\sim 10\ \mathrm{GeV}$, unless the mass splitting is large enough so that the up-scattering process is forbidden. For a higher mass, there are parameter regions where the model evades the core-collapse constraints while the inelastic scattering is kinematically allowed. This work demonstrates that astrophysical observations can provide powerful tests for inelastic dark matter models with a light mediator. The analysis can be used to constrain models where dark matter is made of a composite state, such as dark atoms and nuclei. It is also interesting to test those models using observations of galaxy clusters that show evidence of a density core in their inner halos [102, 103].

Additionally, if there are portals connecting the dark matter sector to the standard model, this scenario may have important ramifications for terrestrial detection experiments. For example, it could produce distinct signals in direct detection experiments, because the mediator mass is comparable to or less than recoil energies and scattering with the target is inelastic. The mediator may also lead to formation of SIDM bound states that could be probed at particle colliders [104]. Furthermore, the mass splitting in the inelastic dark matter model has relevant signatures that could be tested in present and future high-intensity fixed target experiments, see [105]. These interesting topics are left for future work.

CHAPTER 3

DENSITY SPIKES NEAR BLACK HOLES IN SELF-INTERACTING DARK MATTER HALOS AND INDIRECT DETECTION CONSTRAINTS

Indirect searches of high-energy standard model particles originating from dark matter annihilations or decays provide an important way of understanding its nature. Of central importance to the indirect detection search is the distribution of dark matter within galactic halos. In the prevailing scenario of dark matter, it is composed of collisionless thermal relics. Numerical simulations show that collisionless dark matter (CDM) typically produces a Navarro-Frenk-White (NFW) density profile in the halo [106, 107], which has a characteristic feature of $\rho(r) \propto r^{-1}$ towards the center [108]. It has also been established that virtually all large galaxies host central supermassive black holes, see, e.g. [109]. The presence of a central black hole could alter the dark matter density profile in the inner halo, and for the standard NFW profile a density spike, $\rho(r) \propto r^{-7/3}$, could form near a black hole that grew adiabatically [110]. The high density of the spike could boost the dark matter annihilation rate. For example, the Milky Way hosts a central supermassive black hole with mass $\sim 4 \times 10^6\ \mathrm{M}_\odot$ [111, 112]. Dark matter annihilations could produce very bright sharp signals that may be visible as a point source in the galactic center, see, e.g., [110, 113, 114, 115, 116, 117, 118]. Refs. [119, 120] show that observations from the M87 galaxy have excluded thermal relic dark matter in the presence of a CDM spike near its $6.5 \times 10^9\ \mathrm{M}_\odot$ black hole.

It's less known observationally whether small dwarf galaxies, like satellite galaxies of the Milky Way, may host central black holes with intermediate masses. Interestingly, one could derive constraints on the central black hole mass in the satellites using dark

matter indirect detection observations. For example, for the thermal relic scenario with an s-wave annihilation cross section, the central black hole mass cannot be higher than $\sim 10^2$–10^3 $\mathrm{M}_\odot$ in Draco [121], the most dense satellite of the Milky Way, otherwise the flux of dark matter annihilation signals would surpass the upper limit from Fermi-LAT gamma-ray observations due to the presence of the density spike induced by the black hole. These limits could be relaxed if the power law of the spike is more mild. This could occur if the black hole grows away from the center of the halo or it does not grow adiabatically from a seed, but being brought in by mergers [122]. In addition, mergers of black holes in the centers of the progenitor halos could erase the density spike [123]. Gravitational scatterings between stars and dark matter particles could also kinetically heat up the spike and reduce its density [124, 125].

In this chapter, we study indirect detection constraints on dark matter spikes in self-interacting dark matter (SIDM), see [53] for a recent review. In this scenario, dark matter has strong self-interactions that can thermalize the inner halo over cosmological timescales [126, 127, 57, 128, 129, 130, 131]. Recent studies show that SIDM is favored for explaining diverse dark matter distributions over a wide range of galactic systems [103, 54, 132, 133, 134, 135, 136, 137, 138, 139], implying that the inner region of dark halos might be indeed thermalized. Ref. [140] uses a conduction fluid model and derives density profiles of SIDM particles bound to a black hole. For a Coulomb-like self-interaction, a central black hole can induce a density spike of $\rho(r) \propto r^{-7/4}$, which is shallower than the CDM one $\rho(r) \propto r^{-7/3}$. We apply these results to Draco, the Milky Way and M87, and derive upper limits on the annihilation cross section. We will show in SIDM Draco could contain central black holes with intermediate masses $\sim 600\ \mathrm{M}_\odot$ as expected in the black hole-host galaxy relation [141], while the halo is still composed of thermal relic dark matter. And the upper limits can be weakened by factors of $\sim 10^7$ and 10^3 for the Milky Way and M87, respectively. We will also show that M87 could be a promising target for probing SIDM

spikes with data from the Event Horizon Telescope (EHT).

3.1 SIDM density spikes near a black hole

We assume dark matter particles in the inner halo follow an isotropic, quasi-equilibrium distribution due to dark matter interactions. A Schwarzschild black hole is located at the center of the halo with a mass of $M_\bullet$, which is much smaller than the total halo mass, but larger than the mass of bound SIDM particles in the spike. Ref. [140] uses a conduction fluid model and derives density profiles of SIDM particles bound to the black hole, which depend on the form of the self-scattering cross section σ. Consider the parameterization $\sigma = \sigma_0(v/v_0)^{-a}$, where σ_0 is the normalization factor, a characterizes the velocity dependence, v is 1D velocity dispersion of the particles in the spike and v_0 is that of outside, the density follows a power law of

$$\rho \propto r^{-(3+a)/4} \tag{3.1}$$

for $r \lesssim r_{\rm bh} = GM_\bullet/v_0^2$, and the corresponding velocity dispersion scales as $v \propto r^{-1/2}$ [140]. With the power law solution, it's easy to see that the energy flux transported out of the spike due to the self-interactions L is independent of radius, as $L \sim NE/t_r$, where $N \sim \rho r^3$ is the number of bound particles per shell, $E \sim v^2$ energy per particle and $t_r = 1/(\sigma\rho v)$ relaxation time. This is the condition to have a steady state near a black hole [142].

We see that the spike density profile becomes steeper as a increases. Since the cross section is more suppressed in the spike for higher a, the transport rate becomes smaller accordingly, resulting in a higher density. The velocity dependence of σ is related to particle physics realizations of SIDM. For example, a scalar dark matter candidate could have a self-coupling that leads to a constant cross section and $a = 0$ over all scales. More generally, there exists a scalar or vector force mediator with a mass of m_ϕ. When $m_\chi v_0 > m_\phi$, the self-scattering is Coulomb-like, i.e., $\sigma \propto v_0^{-4}$ and $a = 4$. In the opposite limit, it's

point-like and $a = 0$. And in the resonant regime for attractive interactions, $\sigma \propto v_0^{-2}$ and $a = 2$. For a given set of mass parameters, a may vary as well. Consider the best-fit model in [103, 143], where $m_\chi \sim 10^3 m_\phi$. For clusters, $v_0 \sim 10^3$ km/s, the model predicts $a = 4$ in both spike and its surrounding regions. For a dwarf halo with $v_0 \sim 100$ km/s, the self-scattering is point-like in the bulk of the halo, but becomes Coulomb-like towards the inner spike as v increases as $r^{-1/2}$. In addition, black hole and halo masses are correlated. Thus observations of SMBHs over different mass scales may provide a unique probe of SIDM models.

As discussed above, the steepest spike density profile predicted in SIDM is $\rho \propto r^{-7/4}$ for $a = 4$, which is slightly shallower than the one predicted in CDM if the hole grows adiabatically, i.e., $\rho \propto r^{-7/3}$. We will show that the small difference in the logarithmic density slope could lead to significantly different constraints from indirect detection as the signal strength is $\propto \rho^2(r)$. We note that CDM could have a spike profile of $\rho \propto r^{-3/2}$ [110]. Frequent gravitational scatterings between stars near the black hole and CDM particles could drive the latter to follow an isothermal distribution [124, 125]. This effect could be important for the Milky Way, but it's negligible for Draco and M87, as we will discuss later.

To study implications of the density spikes on indirect detection constraints, we need to further specify inner boundary conditions. For SIDM, we extend the spike profile in Eq. 3.1 to 4 $r_\bullet$ where $r_\bullet = 2GM_\bullet/c^2$ is the Schwarzschild radius and set $\rho(4r_\bullet) = 0$. For CDM, we consider annihilation radius $r_{\rm ann}$ that is calculated iteratively as $\rho(r_{\rm ann}) = m_\chi / \langle \sigma_{\rm ann} v_{\rm rel} \rangle t_{\rm age}$ [144, 145], where $\langle \sigma_{\rm ann} v_{\rm rel} \rangle$ is the thermally averaged annihilation cross section and $t_{\rm age} = 10$ Gyr is the age of the system. The CDM spike density saturates to $\rho(r_{\rm ann})$ at the annihilation radius, and we further set $\rho(r) = 0$ for $r \leq 4r_\bullet$ [110] for CDM as in the SIDM scenario. Note in SIDM, dark matter self-interactions could wash out the annihilation plateau [145].

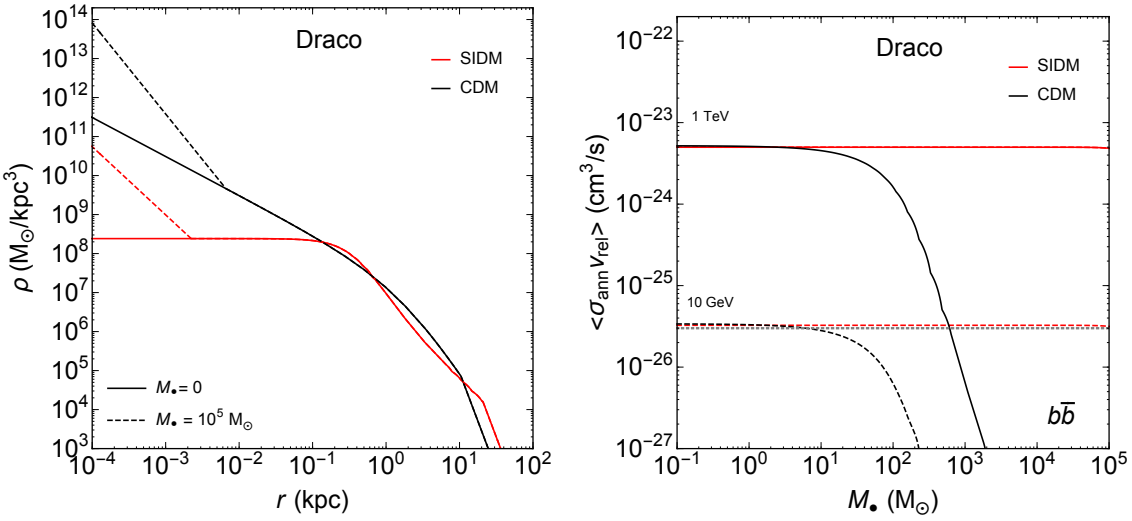

Figure 3.1: *Left:* dark matter halo density profiles for SIDM (red) and CDM (black) halo models for the Milky Way satellite galaxy Draco without (solid) and with (dashed) a central black hole. For the latter case, the black hole mass is assumed to be $10^5\ \mathrm{M}_\odot$ and the density spike follows a power law of $r^{-7/4}$ and $r^{-7/3}$ for the SIDM and CDM halos, respectively. A steep cutoff at around $10\ \mathrm{kpc}$ is due to tidal stripping. *Right:* upper limits on the annihilation cross section vs. the central black hole mass for the SIDM (red) and CDM (black) halos with density spikes, based on Fermi-LAT gamma-ray observations of Draco. The dark matter mass is $10\ \mathrm{GeV}$ (dashed) and $1\ \mathrm{TeV}$ (solid). The horizontal line denotes the canonical thermal annihilation cross section $\langle\sigma_{\rm ann}v_{\rm rel}\rangle = 3\times10^{-26}\ \mathrm{cm}^3/\mathrm{s}$ (dotted gray).

3.2 Applications to Draco

The presence of dark matter spikes could significantly boost indirect detection signals. In turn, if we assume dark matter is made of thermal relics, we can derive constraints on the mass of central black holes of galaxies using results from dark matter indirect searches. Ref. [121] considers Draco, the most dense satellite of the Milky Way, and shows its black hole mass cannot be larger than 10^2–$10^3\ \mathrm{M}_\odot$ for the dark matter mass in the range $100\ \mathrm{GeV}$–$1\ \mathrm{TeV}$, based on the Fermi-LAT gamma-ray data.

Since the SIDM halo model predicts a shallower density spike than the CDM one, we expect that the upper limits on $M_\bullet$ for Draco could be relaxed accordingly. To see the difference, we first consider dark matter density profiles for Draco without a black hole.

Ref. [134] fits the line-of-sight stellar velocity dispersion of Draco with an NFW profile and finds the best-fit values of the scale density and radius are $\rho_s \approx 1.68 \times 10^7\ \mathrm{M}_\odot/\mathrm{kpc}^3$ and $r_s \approx 1.94\ \mathrm{kpc}$, respectively. In addition, it also considers a cored isothermal density profile following the solution to the Jeans equation $v_0^2 \nabla^2 \ln \rho = -4\pi G\rho$ with the boundary conditions $\rho(0) = \rho_0$ and $\rho'(0) = 0$, and finds the best fit values $\rho_0 \approx 2.55 \times 10^8\ \mathrm{M}_\odot/\mathrm{kpc}^3$ and $v_0 \approx 13.88\ \mathrm{km/s}$. This isothermal profile was first proposed to model dark matter distributions in an inner SIDM halo [103, 146] and it agrees with N-body simulations remarkably well [147, 133, 148]. The left panel of Fig. 3.1 (solid) shows the dark matter density profiles for Draco inferred from fitting to stellar kinematics as in [134], where we have extrapolated them for $r \gtrsim 10\ \mathrm{kpc}$ using a power law of r^{-5} to account for tidal stripping.

We use $\rho_{\rm spike}(r) = \rho(r_{\rm spike})\,(r_{\rm spike}/r)^\gamma$ to model the spike density profile, where $r_{\rm spike}$ is the spike radius, and $\gamma = 7/4$ and $7/3$ for SIDM and CDM halos, respectively. For SIDM, we set the spike radius to be the radius of influence calculated as $r_{\rm bh} = GM_\bullet/v_0^2$, where v_0 is the 1D velocity dispersion outside of the spike. It's important to note that v_0 is a constant over the radius for an SIDM halo and the calculation of $r_{\rm bh}$ is self-consistent. Taking $M_\bullet = 10^5\ \mathrm{M}_\odot$ as an example and $v_0 \approx 14\ \mathrm{km/s}$ for Draco [134], we find $r_{\rm spike} \approx 2.2\ \mathrm{pc}$ and $\rho(r_{\rm spike}) \approx 2.4 \times 10^8\ \mathrm{M}_\odot/\mathrm{kpc}^3$ as shown in the left panel of Fig. 3.1 (dashed red). For CDM, v_0 is not a constant and it depends on radius. In this case, we follow [125] and adopt a practical definition of $r_{\rm bh}$ through the condition

$$4\pi \int_0^{r_{\rm bh}} dr r^2 \rho(r) = 2M_\bullet, \tag{3.2}$$

and the CDM spike radius is given by $r_{\rm spike} \approx 0.2 r_{\rm bh}$ [149]. For $M_\bullet = 10^5\ \mathrm{M}_\odot$, we have $r_{\rm bh} \approx 33\ \mathrm{pc}$, hence $r_{\rm spike} \approx 6.6\ \mathrm{pc}$ and $\rho(r_{\rm spike}) \approx 4.6 \times 10^9\ \mathrm{M}_\odot/\mathrm{kpc}^3$; see the left panel of Fig. 3.1 (dashed black). Note the annihilation radius is much smaller than the spike radius

and we do not show it in the figure. For instance, consider $\langle\sigma_{\rm ann}v_{\rm rel}\rangle = 3\times10^{-26}\ {\rm cm}^3/{\rm s}$ and $m_\chi = 100\ {\rm GeV}$, we find $r_{\rm ann}\approx 10^{-4}\ {\rm pc}$ for the CDM halo.

We consider dark matter annihilations to $b\bar{b}$ states, which further produce gamma-ray signals. The differential flux from the contribution of the smooth halo component can be calculated as

$$\frac{d\Phi_{\rm halo}}{dE} = \frac{1}{2}\frac{\langle\sigma_{\rm ann}v_{\rm rel}\rangle}{4\pi m_\chi^2}\frac{dN}{dE}\bar{J} \tag{3.3}$$

where dN/dE is the photon spectrum and $\bar{J}$ is the angular integrated J factor given by

$$\bar{J} = 2\pi\int_0^{\theta_{\rm max}} d\theta\sin\theta J(\theta) = 2\pi\int_0^{\theta_{\rm max}} d\theta\sin\theta\int_{l.o.s} ds\rho^2[r(\theta,{\rm s})]. \tag{3.4}$$

To perform the integral along the line of sight direction, we write $r(s,\theta) = \sqrt{D^2+s^2-2sD\cos(\theta)}$, where $D\approx 76\ {\rm kpc}$ is the distance from Earth to Draco, and we set $\theta_{\rm max} = 0.5^{\rm o}$, corresponding to a solid angle of $2.4\times10^{-4}\ {\rm sr}$. For the SIDM and CDM halos of Draco shown in the left panel Fig. 3.1 (solid), we find $\bar{J}\approx 5.0\times10^{18}\ {\rm GeV}^2/{\rm cm}^5$ and $4.8\times10^{18}\ {\rm GeV}^2/{\rm cm}^5$, respectively. We see that although the two halo models have very different inner density profiles, their $\bar{J}$ factors are similar.

For the contribution from the density spike, we have

$$\frac{d\Phi_{\rm spike}}{dE} = \frac{1}{2}\frac{\langle\sigma_{\rm ann}v_{\rm rel}\rangle}{m_\chi^2 D^2}\frac{dN}{dE}Q, \tag{3.5}$$

where the Q factor is calculated as

$$Q = \int_{r_{\rm min}}^{r_{\rm spike}} drr^2\rho^2_{\rm spike}(r) = \begin{cases}\rho^2(r_{\rm spike})r^3_{\rm spike}\left(\frac{r_{\rm spike}}{r_\bullet}\right)^{1/2}, \text{ SIDM}\\ \frac{3}{5}\rho^2(r_{\rm spike})r^3_{\rm ann}\left(\frac{r_{\rm spike}}{r_{\rm ann}}\right)^{14/3}, \text{ CDM}\end{cases} \tag{3.6}$$

where $r_{\rm min}$ is $4r_\bullet = 8GM_\bullet/c^2$ for SIDM and the annihilation radius $r_{\rm ann}$ for CDM. The

annihilation radius can be calculated as $r_{\rm ann} = [\langle\sigma_{\rm ann}v_{\rm rel}\rangle\, t_{\rm age}\rho(r_{\rm spike})/m_\chi]^{3/7} r_{\rm spike}$. The small volume and saturated density in the annihilation plateau give no significant contribution to the annihilation signal, therefore we ignore it here. In eq. 3.6 we also assume that $r_{\rm min} \ll r_{\rm spike}$ which is reasonable for the Draco system for both SIDM and CDM. For a given dark matter mass, black hole mass and annihilation cross section, we can calculate the expected signal flux by integrating Eqs. 3.3 and 3.5 for $100\ {\rm MeV} \leq E \leq 100\ {\rm GeV}$, the energy range of the Fermi-LAT gamma-ray space telescope. We take the photon spectrum dN/dE from [150, 151], and obtain the total flux as $\Phi_{\rm total} = \Phi_{\rm halo} + \Phi_{\rm spike}$. For $b\bar{b}$ final states, the upper limit on the gamma-ray flux is $\Phi_{\rm upper} \approx (62\text{–}5.8) \times 10^{-11}\ {\rm cm^{-2}s^{-1}}$ for $m_\chi = 10\ {\rm GeV}$–$1\ {\rm TeV}$ [121], based on Fermi-LAT data on Draco. We vary the black hole mass and the dark matter mass, and derive upper limits on the annihilation cross section for the SIDM and CDM halo models of Draco.

The right panel of Fig. 3.1 shows the upper limits on the annihilation cross section vs. the black hole mass for the SIDM (red) and CDM (black) halos, where we consider the dark matter mass $m_\chi = 10\ {\rm GeV}$ (dashed) and $1\ {\rm TeV}$ (solid). The gray horizontal line denotes the canonical thermal cross section $\langle\sigma_{\rm ann}v_{\rm rel}\rangle = 3 \times 10^{-26}\ {\rm cm^3/s}$. For the CDM halo, the thermal relic dark matter is excluded for $m_\chi = 10\ {\rm GeV}$ and $1\ {\rm TeV}$ if $M_\bullet \gtrsim 10\ {\rm M_\odot}$ and $10^3\ {\rm M_\odot}$, respectively. For the SIDM halo, the upper limits on the annihilation cross section are essentially independent of the black hole mass, and the constraints are significantly relaxed. Since both halo models have similar $\bar{J}$ factors for the smooth component, the difference in the $M_\bullet$ bounds is caused by their different spike profiles. Observationally, it's unknown whether Draco has a massive central black hole. If we extrapolate the black hole-host galaxy relation [141] to Draco, it could host a black hole with $M_\bullet \sim 600\ {\rm M_\odot}$. In this case, SIDM could be composed of thermal relics, but CDM could not be for $m_\chi \lesssim 1\ {\rm TeV}$. In the limit where the spike is negligible, our analysis shows thermal relic dark matter is allowed for both halo models with $m_\chi \sim 10\ {\rm GeV}$. Ref. [121] finds a stronger limit

of $m_\chi \gtrsim 30$ GeV for a CDM halo. This is because it considers a density profile with $\bar{J} \approx 1.20 \times 10^{19}\ \mathrm{GeV}^2/\mathrm{cm}^5$, which is a factor of 2.5 higher than our case.

SIDM predicts a weaker density spike near a central black hole. For the satellite galaxies like Draco, the presence of such a spike does not strengthen constraints on the SIDM annihilation cross section unless the black hole mass is much larger than $10^7\ \mathrm{M}_\odot$, which is impossible for those systems given their small masses. As estimated in [135], the halo mass of Draco is about $2 \times 10^8\ \mathrm{M}_\odot$ with a $4 \times 10^9\ \mathrm{M}_\odot$ progenitor falling into the tidal field of the Milky Way. In this work, we focus on dark matter annihilations to $b\bar{b}$, as it is one of the most studied channels in dark matter indirect detection, but it's straightforward to extend to other channels as well. In addition, we could interpret our results in terms of a specific particle physics model of SIDM, combining with other constraints, see. e.g., [58, 152, 153, 154, 155, 156, 157, 158, 159]. It is also interesting to note that Draco was considered as a challenging case for SIDM [160, 161] as it has the highest dark matter content among the Milky Way satellites, but both dark matter self-interactions and tidal interactions are commonly expected to produce a shallow density core for a satellite galaxy. Recent works show the interplay of the two effects could actually lead to an opposite consequence, resulting in a high central density, due to the onset of SIDM core collapse [162, 135, 136, 163, 164]. Ref. [135] uses N-body simulations and demonstrates that the isothermal density profile of Draco shown in the left panel of Fig. 3.1 can be produced in SIDM.

3.3 Implications for the Milky Way and M87

We consider the Milky Way, which hosts a central black hole mass with $M_\bullet \sim 4 \times 10^6\ \mathrm{M}_\odot$ [111, 112]. Such a massive black hole could significantly enhance the spike density and boost indirect detection signals accordingly. Taking Fermi-LAT observations of the Galactic Center in gamma rays, Ref. [165] derives stringent upper limits on the annihila-

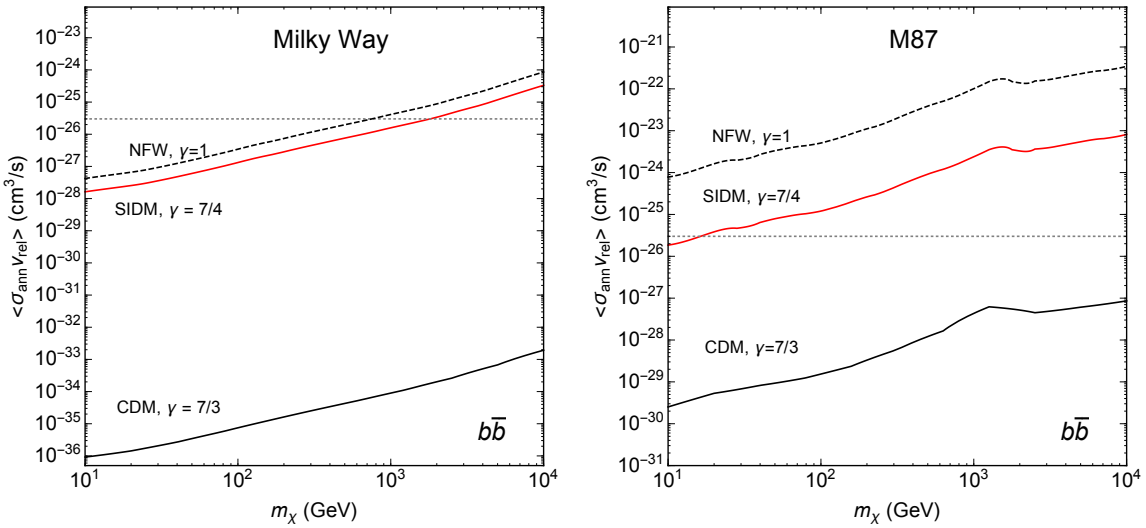

Figure 3.2: *Left:* upper limits on the annihilation cross section for the Milky Way with a central black hole mass of $M_\bullet = 4 \times 10^6\ \mathrm{M}_\odot$ in the presence of SIDM (solid red) and CDM (solid black) spikes, compared to the case assuming a pure NFW halo (dashed black) from [165]. *Right:* similar to the left panel, but for the M87 galaxy with $M_\bullet = 6.5 \times 10^9\ \mathrm{M}_\odot$. The NFW and CDM limits are from [119]. For both panels, the horizontal line denotes the canonical thermal annihilation cross section $\langle \sigma_{\rm ann} v_{\rm rel} \rangle = 3 \times 10^{-26}\ \mathrm{cm}^3/\mathrm{s}$ (dotted gray).

tion cross section for a pure NFW profile and finds $\langle \sigma_{\rm ann} v_{\rm rel} \rangle \lesssim 4 \times 10^{-28}$–$9 \times 10^{-25}\ \mathrm{cm}^3/\mathrm{s}$ for $m_\chi \approx 10\ \mathrm{GeV}$–$10\ \mathrm{TeV}$ and the $b\bar{b}$ channel. We recast these limits to constrain $\langle \sigma_{\rm ann} v_{\rm rel} \rangle$ in the presence of a density spike near the black hole for in both SIDM and CDM. In our study, we demand that the predicted signal flux with a spike should not exceed the one expected from a pure NFW halo as in [165].

We first calculate the normalization factor for the flux. We assume an NFW density profile for the Milky Way halo with $r_s = 26\ \mathrm{kpc}$ and $\rho_s = 4.1 \times 10^6\ \mathrm{M}_\odot/\mathrm{kpc}^3$, consistent with the mean values used in [165]. The $\bar{J}$ factor takes the form $\bar{J} = \int d\ell db \int_{l.o.s.} ds \rho^2[r(\ell, b, s)]$ where b and ℓ are Galactic latitude and longitude, respectively, and $r(\ell, b, s) = \sqrt{D^2 + s^2 - 2sD\cos(\ell)\cos(b)}$ with $D = 8.25\ \mathrm{kpc}$. We integrate both b and ℓ from -20° to 20°, in accord with the signal region in [165], and find $\bar{J} = 2.9 \times 10^{22}\ \mathrm{GeV}^2/\mathrm{cm}^5$. For a given dark matter mass, we take the corresponding upper limit on

$\langle\sigma_{\rm ann}v_{\rm rel}\rangle$ from [165] and convert it into an upper limit on the differential gamma-ray flux using Eq. 3.3.

Unlike Draco, the stellar mass dominates the inner regions of the Milky Way and SIDM thermalization with a deep baryonic potential could lead to a high density with a negligible core size [146], as dense as an NFW halo; see [166] for an example. Thus we can approximate the Milky Way halo in SIDM with the NFW profile for $r \geq r_{\rm spike}$ and match it with the spike $\rho(r) \propto r^{-7/4}$ for $4r_\bullet < r < r_{\rm spike} = r_{\rm bh} = GM/v_0^2$, where we estimate the 1D velocity dispersion as $v_0 = v_{\rm max}/\sqrt{3}$ and $v_{\rm max} = 1.64 r_s\sqrt{G\rho_s}$ [103]. The presence of the stellar mass could further increase v_0, resulting in smaller $r_{\rm bh}$. Thus our estimation of v_0 could lead to a conservative limit on $\langle\sigma_{\rm ann}v_{\rm rel}\rangle$. We then calculate the Q factor given in Eq. 3.6 for the SIDM spike. For CDM, we follow the procedure discussed for Draco to calculate the spike density and radius. For $4r_\bullet < r < r_{\rm spike}$, we take the inner profile to be the geometric mean between the annihilation density and the spike density, i.e., $\rho_{\rm spike}(r)\rho(r_{\rm ann})/[\rho(r_{\rm spike}) + \rho(r_{\rm ann})]$; for $r \leq 4r_\bullet$, $\rho(r) = 0$ [110]. For the Milky Way, we find $r_{\rm spike} = 1.7$ pc and 20 pc for SIDM and CDM spikes, respectively.

The left panel of Fig. 3.2 shows the upper limits on the annihilation cross section from the Milky Way after taking into account SIDM (solid red) and CDM (solid black) spikes, compared to the ones assuming a pure NFW halo (dashed black) from [165]. For SIDM, the presence of the SMBH has a mild effect and only increases the upper limits on $\langle\sigma_{\rm ann}v_{\rm rel}\rangle$ by order unity. In the presence of a CDM spike, the limits are a factor of 10^8 stronger, compared to the pure NFW case. Thus the thermal relic scenario is ruled out for the entire mass range in CDM, while it's allowed for $m_\chi \gtrsim 2$ TeV in SIDM. For a CDM spike of $\rho(r) \propto r^{-3/2}$, caused by dynamical heating by stars, we find the limits are similar to the SIDM ones.

Lastly, we consider the supergiant elliptical galaxy M87, which hosts a central black hole mass with $M_\bullet \approx 6.5 \times 10^9$ M$_\odot$ [167, 168]. Ref. [119] assumes a spike with $\rho(r) \propto$

$r^{-7/3}$ for M87, and derives upper limits on the annihilation cross section to $b\bar{b}$ as $\langle\sigma_{\rm ann}v_{\rm rel}\rangle \lesssim 6\times10^{-30}$–$10^{-26}$ $\rm cm^3/s$ for the dark matter mass in a range of $m_\chi \approx 10$ GeV–100 TeV, a factor of 10^6 stronger compared to a pure NFW halo. Thus, for CDM, thermal relic dark matter has been excluded for the entire mass range for M87. Compared to the Milky Way, M87 is dynamically young and the CDM spike is expected to survey as gravitational heating is insufficient [119].

We recast the limits to the case with an SIDM spike, using the approach for the Milky Way discussed previously. For the M87 halo, we take the NFW parameters $r_s = 20$ kpc and $\rho_s = 6.6\times10^6\ \rm M_\odot/kpc^3$ following [119]. The right panel of Fig. 3.2 shows the upper limits on the annihilation cross section from M87 after taking into account SIDM (solid red) and CDM (solid black) spikes [119]. For SIDM, the presence of the SMBH increases the upper limits on $\langle\sigma_{\rm ann}v_{\rm rel}\rangle$ by a factor of ~ 80, compared to the case with a pure NFW halo (dashed black). For a CDM spike, the limits are a factor of 10^5 stronger. Thermal relic scenario is excluded in CDM, while it's allowed for $m_\chi \gtrsim 20$ GeV in SIDM. This lower bound is weaker than the Milky Way one, $m_\chi \gtrsim 2$ TeV.

Another exciting aspect about the M87 target is that the EHT could resolve the dark matter density profile near the hole, due to its unprecedented angular resolution. Ref. [120] shows the EHT is sensitive to synchrotron emission induced by dark matter annihilations and the radiation from the annihilations could further enhance the photon ring around the shadow of the black hole. For a CDM spike with the $b\bar{b}$ channel, it shows $\langle\sigma_{\rm ann}v_{\rm rel}\rangle \lesssim 3\times10^{-31}$ for $m_\chi \approx 10$ GeV, based on previous data releases from the EHT collaboration [169, 170]. We estimate the EHT sensitivity as $\langle\sigma_{\rm ann}v_{\rm rel}\rangle \lesssim 5\times10^{-28}\ \rm cm^2/s$ with $m_\chi \approx 10$ GeV for an SIDM spike, which is comparable to the upper limit from the Milky Way; see the left panel of Fig. 3.2. Thus the EHT provides an interesting test of thermal SIDM models. Recently, the EHT collaboration observed the black hole shadow of M87 for the first time [168]. It would be of interest to take their new results and further test the nature

of dark matter, which we leave for future work.

3.4 Summary

Dark matter density spikes may form in the presence of a central black hole in galaxies. This work has studied indirect detection constraints on dark matter annihilations after taking into account spikes predicted in SIDM and CDM models. For Draco, the upper limits on the cross section are not sensitive to the presence of an SIDM density spike ($\rho \propto r^{-7/4}$), if the black hole mass is reasonable for the system we consider. In contrast, the possibility of an existing intermediate black hole in Draco has been excluded for thermal relic CDM, as it predicts a steeper spike profile ($\rho \propto r^{-7/3}$). This work further studied constraints from the Milky Way and M87, which host central supermassive black holes, and found that the upper limits on the annihilation cross section can be significantly weakened in SIDM. Observations from both galaxies exclude a thermal relic scenario for CDM for s-wave annihilations, but it's still allowed for SIDM. In addition, EHT observations of the M87 black hole can further probe the presence of an SIDM spike. In the future, the distribution of SIDM particles near a black hole in the strong gravitational limit, which might be important for understanding growth of supermassive black holes in the early Universe, see., e.g., [171, 172, 94], could be studied.

CHAPTER 4

HEATING OF NEUTRON STARS WITH RELATIVISTIC TARGETS BY INELASTIC DARK MATTER

Inelastic dark matter models such as those discussed in Chapter 2 are a class of well motivated models [173, 68] that were initially proposed to address the DAMA annular modulations [174]. These models generally consist of two dark matter mass states with small mass splitting (δm) between them. This is a generic arrangement that can occur in various models. For example, it occurs in the case presented in Chapter 2 of dark photon mediated pseudo-Dirac dark matter. In the case of dominant off-diagonal coupling compared to the diagonal, the terrestrial direct detection limits are severely weakened if the universe is populated by lighter state of the dark matter. These limits disappear for relative mass splitting greater than 10^{-6} GeV as there is not enough kinetic energy available in the dark matter particle hitting the detector at $\mathcal{O}(10^{-3})$ km/s to scatter to a heavier state.

This is no longer the case when the particle can be accelerated to relativistic velocities. Terrestrially this could be achieved by particle accelerators. In this case inelastic dark matter can be searched in displaced vertices at the colliders or at the fixed target experiments. High-intensity experiments such as B-factories are good at probing the parameter space involving mediator masses < 10 GeV. For probing the parameter space with heavier mediators existing (ATLAS, CMS, LHCb) and proposed (CODEX-b, FASER, MATHUSLA) experiments at the LHC are more suited [175].

Alternatively, another attractive possibility is to use the accelerators in the sky namely Neutron Stars (NS). Since the escape velocity from the surface of a NS is about $0.6\,c$, the infalling dark matter from the halo is accelerated to relativistic speeds when it passes through

a NS. This large kinetic energy can allow it to jump the mass gap which could facilitate inelastic scattering. The kinetic energy lost during scattering can heat up a cold NS from $\mathcal{O}(100)$ K temperature to $\mathcal{O}(1000)$ K, temperature.

If next generation radio telescopes such as FAST [176], CHIME [177], SKA [178] can detect a nearby $\mathcal{O}(10)$ parsec far $\mathcal{O}(10^9)$ year old NS, which should have $\mathcal{O}(100)$ K temperature in absence of dark heating, then upcoming infrared telescopes like JWST [179], TMT [180], EELT [181] could be pointed towards it which could reveal heating of the star to $\mathcal{O}(1000)$ K temperature. This possibility has been explored in [182, 183]. In particular the effect of inelastic dark matter that couples to nucleons has been studied previously in the EFT framework [184].

In this work, we study the competing constraints on inelastic dark matter due to NS kinetic heating with those due to terrestrial experiments. First we show generic projected bounds on a vector mediated inelastic dark matter due to NS for both heavy and light mediator cases for fixed mass splitting as well as fixed relative mass splitting. We then consider a specific benchmark model of dark photon mediated pseudo-Dirac dark matter model to compare and show the complementarity of NS projected bounds with terrestrial accelerator and beam dump experiments.

The dark matter could also be leptophilic, in which case its scattering with the electrons and muons in the NS plays a dominant role in the capture. Since electrons in the NS are ultra-relativistic, this needs a full relativistic calculation of the dark matter capture. In the case of elastic dark matter this has been done previously [185]. In this work we extend the approach in [185] to the case of inelastic dark matter. All of the projected constraints mentioned in the previous paragraph are computed for electron targets.

In section 4.1, we briefly discuss the kinematics of the vector mediated NS heating by inelastic dark matter. In section 4.2, we present the projected bounds due to NS kinetic heating due to generic inelastic dark matter for 6-dim vector-vector contact operators and

light vector mediators for spin-1/2 dark matter. We also compare them with terrestrial direct detection experiments. In section 4.3, we evaluate the NS bounds on specific benchmark models that are theoretically and cosmologically interesting. We show the NS bounds on dark photon mediated pseudo-Dirac dark matter models for fixed ratios of m_ϕ/m_χ. We compare them with the reach of terrestrial direct detection as well as current and future collider and beam dump experiment bounds. Another astrophysically interesting class of models is SIDM models. We show coupling sensitivity for vector mediated inelastic SIDM models that are impossible to detect in current or future direct detection experiments, but can be readily probed with NS heating. Concluding remarks and a discussion on the uncertainties are found in section 4.4.

4.1 Kinematics of Neutron Star Heating

The kinematics of NS heating for contact interactions in case of all dim-5 and dim-6 effective operators for spin-0 and spin-1/2 elastic dark matter was explored in [185]. Kinematics for light vector mediated interactions of elastic dark matter was explored previously in [186]. Inelastic kinetic heating due to scattering of spin-1/2 heavy dark matter with nucleons via contact interactions was first discussed in [184]. We briefly summarize it in this section before extending it to the inelastic dark matter capture. The scalings on mass scales emerging from this analysis will help explain the features in the results summarized in the next section.

In this section, we assume (i) a generic simplified dark matter model consisting of two species χ_1 and χ_2 of masses m_1 and m_2 respectively, separated by a small mass δm with $m_1 < m_2$, (ii) a vector portal to allow the interaction between the visible and dark sectors, (iii) predominant couplings of the dark matter with the portal are off-diagonal thus making the inelastic scattering a primary detection mode of such dark matter, (iv) the dark matter

$m_{\rm T}$	Non-Relativistic		Relativistic			
m_{χ_1}	Heavy	Light	Heavy	Light-ish	Med. Light	Very Light
$\delta m_{\rm max}$	$(\gamma_{\rm esc}-1)m_{\rm T}$	$(\gamma_{\rm esc}-1)m_{\chi_1}$	$p_{\rm F}$	$(\gamma_{\rm esc}-1)m_{\chi_1}$	$(\gamma_{\rm esc}-1)m_{\chi_1}$	$(\gamma_{\rm esc}-1)m_{\chi_1}$

Table 4.1: The values of $\delta_{\rm max}$ as per Eq. 2.4 up to the lowest order. The values obtained in non-relativistic target case match $\delta_{\rm max}$ evaluated in previous study of inelastic dark matter capture in NS with non-relativistic targets [184].

relic density in the universe predominantly consists of the lighter of two species of dark matter.

Under these assumptions, the $\chi_1\, T \rightarrow \chi_2\, T$ is the predominant scattering mode for the dark matter to get captured in a celestial object via scattering with target particles T inside the star. The strong gravitational field of a NS means the dark matter can attain $\gamma_{\rm esc} \sim 1.25$ at the surface of the NS [185]. If the dark matter particle can lose kinetic energy greater than its kinetic energy in the halo during the transit through the star then it can get gravitationally bound to the star and said to be captured. Deposited kinetic energy can heat up a star of radius $R_\star = 12.6$ km and mass $M_\star = 1.5\ M_\odot$ up to 1600 K. The capture efficiency (f) dependence of the temperature is given as [182, 183]

$$T = 1600\, f^{1/4}\, \text{K}. \tag{4.1}$$

We adapt the capture efficiency calculation of [186] for the inelastic dark matter case. Invariance of total energy in Center of Momentum (CM) frame ($\sqrt{s} = E_{\rm CM}$) allows us to calculate the magnitude of the momentum of dark matter final state in the CM frame ($k'_{\rm CM}$) to be

$$k'^2_{\rm CM} = k^2_{\rm CM} - \frac{(m_2^2 - m_1^2)(2E^2_{\rm CM} + 2m^2_{\rm T} - m_1^2) - m_2^2}{4E^2_{\rm CM}} \tag{4.2}$$

Here $k_{\rm CM}$ is the magnitude of initial dark matter momentum in the CM frame. In the case of inelastic dark matter, the energy transferred to the target in the NS frame can be written

as

$$\begin{aligned}\Delta E_{\rm NS} = \; & \gamma\left(\sqrt{m_1^2+k_{\rm CM}^2}-\sqrt{m_1^2+k_{\rm CM}'^2}\right)+\gamma\left(\boldsymbol{\beta}\cdot\mathbf{k}_{\rm CM}\right)\left(1-\frac{k_{\rm CM}'}{k_{\rm CM}}\cos\psi\right)\\ & -\frac{k_{\rm CM}'}{k_{\rm CM}}\gamma\sqrt{\beta^2k_{\rm CM}^2-\boldsymbol{\beta}\cdot\mathbf{k}_{\rm CM}}\sin\psi\cos\alpha,\end{aligned} \tag{4.3}$$

where ψ and α are the polar and azimuthal angles of scattering in the CM frame. In this section we will only discuss the key deviations from the elastic case.

It is important to note where the inelastic scattering departs from the elastic scattering. The momentum and energy transferred is saturated for dark matter masses greater than 1 GeV [186] in case of both non-relativistic and relativistic targets. Since, the requirement that the target must always be knocked out of its Fermi sphere means less percentage of initial kinetic energy available for transition from m_1 to m_2. Maximum kinetic energy available in incoming dark matter is $\sim 0.35\, m_1$. Therefore, the maximum $\Delta = \delta m/m_1$ possible is $(\gamma_{\rm esc}-1)$. This is achieved for $m_1 < 1$ GeV. For $m_1 > 1$ GeV, the kinetic energy transferred is saturated at $(m_{\rm T})p_F$ for (non)-relativistic, so the maximum allowed Δ simply goes as $1/m_1$ as $m_1 \to \infty$. This will lead to a sudden fall in sensitivity of the NS heating probe for heavy dark matter masses when the ratio Δ is fixed. Conversely, if the mass gap $\delta m = m_2 - m_1$ is fixed then the dark matter with heavy masses will always get captured as long as δm is less than the saturation value $\delta m_{\rm max}$.

Conditions on $k_{\rm CM}'$ and $\Delta E_{\rm NS}$ will determine the maximum mass gap that can lead to successful capture at a given dark matter mass. These conditions simply follow from the fact that $k_{\rm CM}'$ should have a real value less than $k_{\rm CM}$ and $\Delta E_{\rm NS}$ should be large enough to knock the target out of its Femi sphere. These facts can be written as

$$0 < k_{\rm CM}'^2 < k_{\rm CM}^2; \quad \Delta E_{\rm NS} + E_p > E_{\rm F} \tag{4.4}$$

Using Eq. 4.2 and Eq. 4.3, and retaining the lowest order terms, we obtain $\delta m_{\rm max}$ that are tabulated in Table 4.1. In the regimes of light dark matter for relativistic targets, we find that the second condition of Eq. 4.4 is the most restrictive, while the first condition sets the value of $\delta m_{\rm max}$ in all the other regimes tabulated in Table 4.1.

The colored regions in the projected bounds shown in the results in the following sections correspond to a temperature of 1600 K. The bounds will not extend to the full $\delta m_{\rm max}$ values tabulated in the respective regimes except in the case of ultra-relativistic targets and heavy dark matter masses. For δm values very close to the maximum allowed value, the kinetic energy transfer is only a fraction of the total kinetic energy of the incoming dark matter. After each successive collision, the dark matter speed is reduced thus reducing the corresponding boost factor. Since the maximum δm allowed is dependent on the dark matter boost factor, for the subsequent collisions the maximum δm is less than the δm present, thus the dark matter never fully thermalizes. This effect causes a slight shift in the falling edge in the projected bounds for heavy dark matter and non-relativistic targets and reduction in the $\Delta_{\rm max}$ for the light dark matter regimes irrespective of the target type if the temperature is fixed to a particular value, such as 1600 K. The only regime unaffected by this effect is that of the heavy dark matter with ultra-relativistic targets as evident from Table 4.1.

4.2 Projected Neutron Star Heating Bounds for Inelastic Dark Matter

We explore the reach for NS heating from inelastic dark matter scattering assuming a generic effective contact operator between fermionic dark matter and standard model fermions. This approach is generic and can apply to scattering between dark matter and any fermionic components of a NS. The reach is shown in Fig. 4.1 for three values of the mass gap $\delta m = 10,\, 100,\, 1000$ keV. The reach is shown for the product of the dark coupling con-

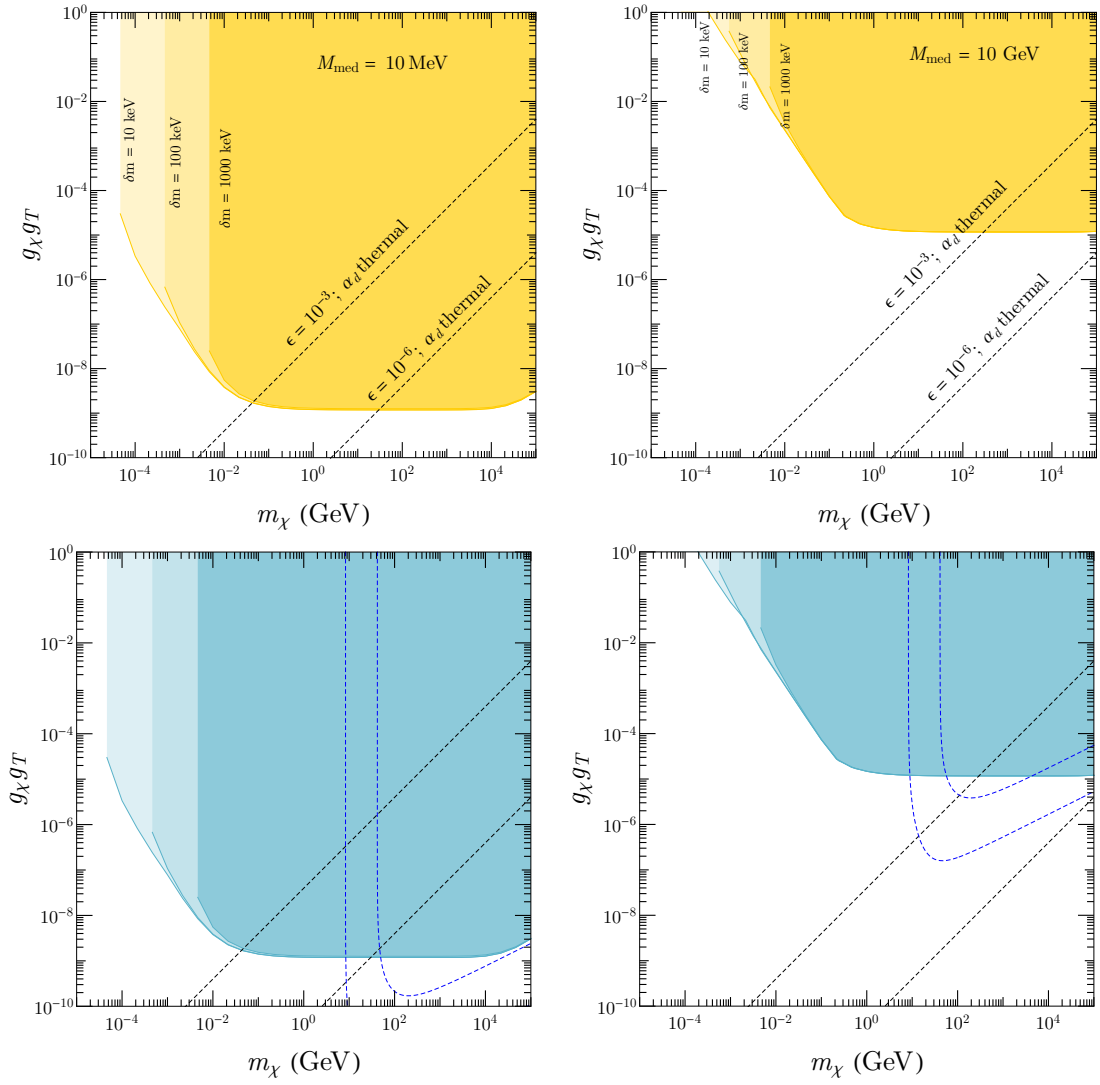

Figure 4.1: NS reach in terms of the product of dark coupling g_χ and the target coupling g_T with fixed mass gaps $\delta m = 10$, 100, 1000 keV. Upper Left : Electron targets with light mediator mass of 10 MeV. Upper Right : Electron targets with heavy mediator mass of 10 GeV. Lower Left: Proton targets with light mediator mass of 10 MeV. Lower Right: Proton targets with heavy mediator mass of 10 MeV. The dotted black shows lines for dark coupling set by the relic density condition $\alpha_\chi = 0.001(m_1/270\ \text{GeV})$ for a kinetic mixing parameter $\epsilon = 10^{-3}$ and 10^{-6}. The dotted blue lines show the terrestrial direct detection limits. There are no direct detection signals for electron targets in this region of parameter space due to kinematics.

stant g_χ and the target coupling constant g_T where the targets are relativistic electrons and protons. The upper left plot shows the NS heating reach for electron targets with a me-

diator mass $m_\phi = 10$ MeV and the upper right plot shows the reach for electron targets with a mediator mass $m_\phi = 10$ GeV. The lower left panel is for proton targets with a light mediator mass of 10 MeV and the lower right panel is for proton targets with a heavy mediator mass of 10 GeV. Also shown are lines for the dark fine structure constant fixed by the thermal relic condition $\alpha_\chi = 0.01(m_1/270\ \mathrm{GeV})$ with values of the kinetic mixing parameter $\epsilon = 10^{-3}$ and 10^{-6}. The dotted blue lines in the lower panels show the terrestrial direct detection limits for proton targets. There are no terrestrial direct detection limits for the electron targets due to kinematics. For details on the terrestrial direct detection limits see Appendix B.

For low dark matter masses we find that the NS kinetic heating reach is limited by Pauli blocking as can be seen in Fig. 4.1. As the mass becomes larger, the reach eventually saturates for a mass above $m_1 = 10^{-2}$ GeV $(1$ GeV$)$ for Fig. 4.1 left (right). For even larger masses we find that the reach begins to become limited again. This is due to the fact that for large dark matter masses multiple scatters are required for the dark matter to be captured, reducing the available phase space. A cut off can be clearly seen in Fig. 4.1 (left) for small masses corresponding to the kinematics related to the value of the mass gap. Since the figure is plotted for a fixed mass gap, smaller dark matter masses require larger velocities to overcome the mass gap. This gives rise to a kinematic suppression which does not allow for up-scattering and therefore no NS heating.

4.3 Benchmark Models

We take a pseudo-Dirac dark matter particle with a light state m_1 and a heavy state m_2 with mass $m_2 = m_1 + \delta m$. The dark matter self-interactions are off diagonal and mediated by a vector mediator m_ϕ. Furthermore, we assume a vector-vector portal between the dark sector and SM particles. We take the standard kinetic mixing scenario between the

dark vector mediator m_ϕ and the SM photon with a mixing parameter ϵ. We assume that the lighter state dark matter is the dominant component as the heavy state dark matter is unstable cosmologically. Interconversions between the two states by the tree level process $\chi_2\chi_2 \to \chi_1\chi_1$ drives the density of the heavy state down [68]. There are scenarios where the above scattering process freezes out when there is a significant abundance of the heavy state χ_2 [187, 188], but here we take as a benchmark model the scenario where the dark matter is composed predominantly of the light state χ_1. The dominant scattering channel is the inelastic up scattering process $\chi_1\chi_1 \to \chi_2\chi_2$ as the elastic scattering $\chi_1\chi_1 \to \chi_1\chi_1$ is loop suppressed due to the off-diagonal nature of the coupling. It should be noted that although the elastic scattering process is loop suppressed the presence of a light mediator can enhance the scattering cross section, thus making the elastic process comparable to the inelastic mode as we found in Chapter 2.

Heavy mediator scenario with fixed Ratio m_ϕ/m_1

If the mediator is lighter than the dark matter then the annihilation to the mediator is a dominant mode for freeze-out of the dark matter. Such reactions are unsuppressed at late times and face stringent constraints from indirect searches [153]. On the other hand, for the heavier mediator case, the freeze-out proceeds through annihilation to SM particles, where the annihilation rate is exponentially suppressed at late times, thus avoiding the indirect detection constraints. Therefore, we project the NS bounds for this cosmologically viable parameter space of dark photon mediator pseudo-Dirac dark matter models with heavy mediators and compare them with terrestrial experiments. Constraints on such models due to current and future accelerator and beam dump experiments have been studied in [175], by fixing the ratio of $m_\phi/m_1 = 3$. Increasing this ratio pushes it towards the region already excluded by BaBar [189] and LSND [190], thus making it cosmologically less interesting.

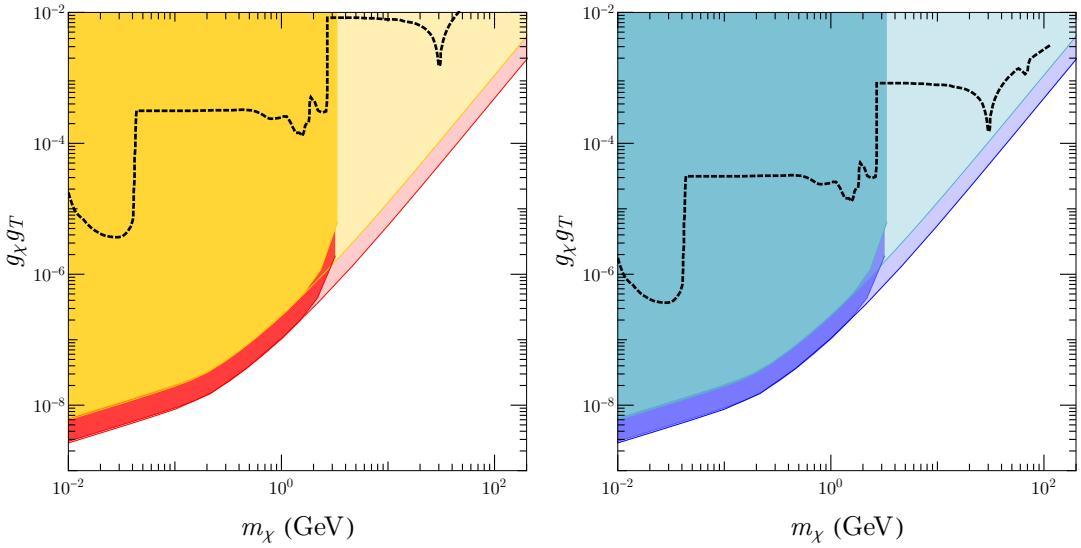

Figure 4.2: The left panel shows limits for electron targets. Yellow: region that can be probed by NS kinetic heating for $m_\phi = 3m_1$. Red: the same but for $m_\phi = 2m_1$. The right panel shows limits for proton targets. Light Blue: region corresponding to $m_\phi = 3m_1$. Dark Blue: region corresponding to $m_\phi = 2m_1$. In both panels the darker shading is for $\Delta = 10^{-1}$ and the lighter shading for $\Delta = 10^{-3}$. Black dashed line: collider and beam dump current and future experiments taken from [175]. The dark fine structure constant is set as $\alpha_\chi = 0.1$.

Additionally, the ratio $m_\phi/m_1 = 2$ leads to resonant enhancement of the annihilation, whose cosmological consequences are explored in [191]. Here we show the NS projected bounds for both well motivated models. Apart from being stronger than the terrestrial experiments, we note another important feature of the NS bounds, that they remain very insensitive to changing the ratio m_ϕ/m_1.

We fix the ratio between the dark vector mediator m_ϕ and the dark matter mass m_1 and compare the NS bounds to bounds from collider and beam dump bounds from current and projected future experiments. For the fixed ratio model we focus on the heavy mediator parameter space where the claim that the inelastic scattering dominates is justified. Fig. 4.2 left shows the NS bounds for electron targets with fixed ratios $m_\phi/m_1 = 3$ (orange) and 2 (red). The right panel is for proton targets with fixed ratios $m_\phi/m_1 = 3$ (dark blue)

and 2 (light blue). In both panels the terrestrial constraints are shown (black dashed). The collider and beam dump bounds for current and projected future direct detection terrestrial experiments are taken from [175]. The darker shaded regions correspond to $\Delta = 10^{-1}$ and the lighter regions for $\Delta = 10^{-3}$. The dark fine structure constant is fixed to a value of $\alpha_\chi = 0.1$. Clearly, the NS bounds for dark matter - electron scattering are superior compared to terrestrial experiments by 2-3 orders of magnitude throughout the explored parameter space.

Self-Interacting Dark Matter

Self-interacting dark matter models typically involve a light mediator between the dark sector and the visible sector. The scattering cross section with light mediators needed to solve the small-scale structure problems like core vs. cusp problem falls into the non-perturbative regime [58]. This requires a non-trivial velocity dependence due to the limits stemming from cluster-size objects. However, these models are strongly constrained by terrestrial direct detection experiments [192, 193]. Additionally, the decay of the light mediator needs to be sufficiently rapid, i.e., before Big Bang nucleosynthesis.

A natural solution to reconcile both requirements are inelastic up-scattering interactions, that are suppressed or even kinematically forbidden in direct detection experiments, provided the mass splitting between the two-states is sufficiently large. The minimum velocity necessary to overcome the mass gap is $\mu_{\chi \mathrm{T}} v_{\mathrm{min}}^2/2 = 2\delta m$ where $\mu_{\chi \mathrm{T}}$ is the reduced mass of the dark matter and target. For typical velocities in the Milky Way $v \sim 300\ \mathrm{km/s}$ and a dark matter mass of $100\ \mathrm{GeV}$, a mass splitting of $\delta m \sim \mathcal{O}(100)\ \mathrm{keV}$ is sufficient to kinematically forbid scattering in terrestrial direct detection experiments. Previous studies [68] numerically solve the Schrodinger equation to find regions in the parameter space of dark matter and mediator masses, for various couplings and mass splittings, where the

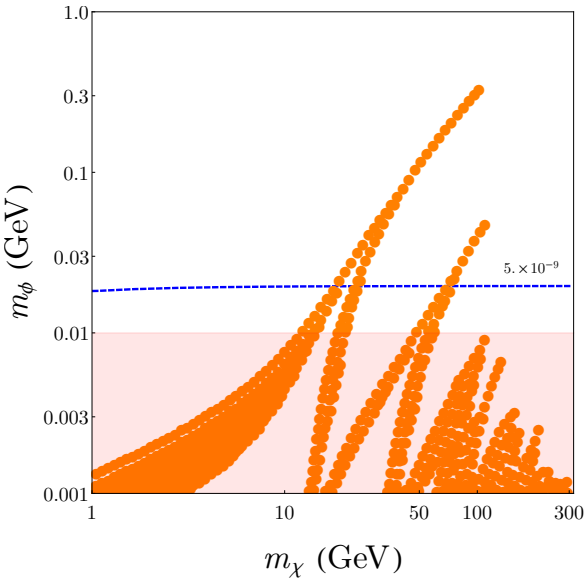

Figure 4.3: The dark orange regions satisfy the small scale structure constraints where $0.5\ \mathrm{cm}^2/\mathrm{g} \leq \sigma_{\chi_1\chi_1\to\chi_1\chi_1}/m_1 \leq 5\ \mathrm{cm}^2/\mathrm{g}$ and have large enough mass gap, $\delta m = 1\ \mathrm{MeV}$, to evade the direct detection constraints from terrestrial experiments. The dark fine structure is fixed at $\alpha_\chi = 0.01$. The pink region is excluded from stellar cooling constraints. Above the blue contour of $\epsilon = 5 \times 10^{-9}$ NS heating is sensitive to the parameter space.

small scale structure problems can be solved, the dark matter has the correct relic abundance and direct detection limits can be evaded. In this section, we show the ability of NS kinetic heating to provide a wide coverage to such regions.

In Fig. 4.3, we show the regions of $m_\chi - m_\phi$ parameter space, where the above three conditions are satisfied and a old NS can be heated to $T_\star = 1600$ K for a value of kinetic mixing $\epsilon = 5 \times 10^{-9}$ indicated by the blue contours. The mass splitting is fixed to $\delta = 1$ MeV, a representative value of mass splitting that could not be probed by current or near future terrestrial direct detection experiments. The dark fine structure constant is fixed to a constant value of 0.01. The cross-section is constrained in the range $0.5\ \mathrm{cm}^2/\mathrm{g} < \sigma_{\chi\chi\to\chi\chi,V} < 5\ \mathrm{cm}^2/\mathrm{g}$. We also show the parameter space excluded by stellar cooling in the pink shaded region taken from [194].

4.4 Summary

The dense environment of a NS makes these compact objects excellent detectors for dark matter - SM interactions. Dark matter in-falling in the steep gravitational well of the NS can be accelerated to relativistic speeds. Scattering between dark matter and the SM components of the NS can impart enough kinetic energy to heat the NS from $\mathcal{O}(100)$ K to $\mathcal{O}(1000)$ K temperatures [182, 183]. The electrons in the NS are ultra relativistic due to their large fermi surfaces. Therefore, a full relativistic treatment of dark matter - electron scattering is needed to calculate the NS heating bounds as in [185, 186]. Models of inelastic dark matter have been proposed to explain the DAMA annual modulation [173] as well as evade direct detection terrestrial constraints [68]. The non-relativistic velocities of dark matter in terrestrial experiments make it kinematically forbidden for inelastic dark matter to be detected for large enough mass gaps. However, NS can easily overcome these mass gaps given the relativistic velocities of the in-falling dark matter. This allows NS heating to probe parameter space which is not possible to probe in present or future terrestrial collider and beam dump experiments.

We calculate the NS heating reach for a generic dim-6 contact operator for fermionic dark matter. Then we calculate the coupling reach for a vector-vector portal between the dark sector and the SM for various relative mass gaps $\Delta = \delta m/m_1$ for both light and heavy dark vector mediator. Finally, we calculate the NS heating bounds for a benchmark model of pseudo-Dirac dark matter with a vector mediator kinetically mixed with the SM photon. We present plots for fixed ratios of the mediator to dark matter mass m_ϕ/m_1 and compare with current and future collider and beam dump bounds taken from [175]. We find that the NS heating bounds are superior to the collider and beam dump bounds by about 2-3 orders of magnitude in the parameter space we explore. We also show that NS heating can probe iSIDM parameter space where small scale structure constraints are satisfied and terrestrial

direct detection bounds are evaded. Neither current nor future terrestrial collider and beam dump experiments are capable of probing this parameter space. Stellar cooling bounds exclude a portion of the parameter space but there remains parameter space which can only be probed using NS heating. A single observation of a $\mathcal{O}(10^9)$ yr aged NS at a temperature of $\mathcal{O}(1000)$ K temperature could be enough to discover particle dark matter or else put strong constraints on particle dark matter models. This is very exciting considering the next generation radio telescopes such as FAST [176], CHIME [177], SKA [178] and upcoming infrared telescopes like JWST [179], TMT [180], EELT [181] which could potentially discover such a NS.

Finally, we note the uncertainties involved in the projected bounds that are shown. Uncertainties associated with the approach in [186, 195, 196, 197] are discussed in those references. They mainly stem from the dark matter velocity distribution, variation in densities and the chemical potential of the contents of the NS near the surface and finally variation in the densities based on EoS. For both relativistic and non-relativistic target species, the assumptions made in [186] give conservative projected bounds on the cut-off by a small $\mathcal{O}(1)$ factor as pointed out in [185]. For projected bounds on the $g_\chi g_{\rm T}$ or ϵ coupling these uncertainties will translate into a larger $\mathcal{O}(1)$ factor, because this quantity goes as the square root of the capture rate unlike the cut-off scale which goes as $1/4^{\rm th}$ power of the capture rate.

Additionally, as pointed out in [198], at high momentum transfer, the fact that the protons are not a free Fermi gas can lead to further order of magnitude correction in capture rate, which implies an additional small $\mathcal{O}(1)$ factor correction in the projected cut-off bounds shown in this work. This effect is in the direction of reducing the reach of NS kinetic heating. Overall the combined effect of all factors put together is a small (large) $\mathcal{O}(1)$ factor uncertainty in the projected bounds for cut-off scale (for $g_\chi g_{\rm T}$ or ϵ) shown here for both electron and proton targets. The main point is that the NS heating can of-

fer to be an independent, complementary and for considerable mass range of dark matter much stronger probe of inelastic as well as SIDM. This core point is independent of the uncertainties mentioned above.

CHAPTER 5
CONCLUSION

The SM of particle physics is arguably one of the greatest achievements of modern physics. It describes nature at a microscopic level to an unprecedented accuracy and makes many predictions of particles which were later discovered experimentally. However, with many unanswered questions about fundamental physics we are required to search for new physics beyond the SM. The open question that this work focuses on is the dark matter problem. Galactic radial velocity curves imply the existence of a non-luminous substance which holds galaxies together gravitationally. The CMB observations further show that about 26% of the universe's matter-energy budget is in the form of this non-luminous matter.

The conservative approach is to assume that dark matter is a new fundamental particle which does not interact with the SM strongly. The zeroth order approximation is to assume that dark matter is collisionless. The collisionless paradigm, although successful on large scales, has problems explaining small scale observation such as the core vs cusp problem. To alleviate the observational tensions between observation and the collisionless dark matter paradigm, self-interaction in the dark matter sector can be introduced. The SIDM paradigm gives rise to rich phenomenology at the astrophysical scale which can be used to probe the particle nature of dark matter.

For pseudo-Dirac dark matter mediated by a U(1) light gauge boson the Majorana mass terms break the dark matter into two mass eigenstates. The mass eigenstates differ in mass by an amount δm introducing an inelastic component to the model. The dark matter self-interactions are off diagonal in nature with a tree level inelastic scattering mode and a loop level elastic scattering mode. Although the elastic scattering occurs at loop level,

the presence of a light mediator enhances the scattering cross section and both modes are present in the halo.

We develop a numerical method to compute both the elastic and inelastic scattering cross sections for this model. We set the dark fine structure constant using the relic abundance relation $\alpha_\chi = 0.01(m_\chi/270\ \mathrm{GeV})$ and then calculate the parameter space that can solve the small scale structure problems with $1 < \sigma_{\mathrm{V}}/m_\chi < 5\ \mathrm{cm}^2/\mathrm{g}$ for a wide range of dark matter masses, $10\ \mathrm{MeV}$–$160\ \mathrm{GeV}$. Additionally, if the heavy state dark matter can decay to a light species that can escape the halo there are constraints coming from halo dynamics. These dissipative interactions can cool the halo speeding up SIDM core collapse on an observationally unfavored time scale. Unless the mass splitting is large enough to kinematically forbid the up-scattering channel, we find that the core collapse time scale strongly constrains this model for dark matter masses below $\sim 10\ \mathrm{GeV}$. For masses above $10\ \mathrm{GeV}$ we find that there is available parameter space that can evade the core collapse constraints for a kinematically allowed up-scattering channel.

This work has demonstrated that halo dynamics can provide strong tests for inelastic SIDM models with a light mediator. These constraints can also be applied to other inelastic models of dark matter such as composite state dark matter such as dark atoms and nuclei. It is also interesting to consider the observational constraints relevant at the cluster scale [102, 103]. Inelastic models of SIDM with a light mediator also have interesting ramifications for terrestrial direct detection experiments. The light mediator could lead to dark matter bound states in particle colliders [104]. The mass splitting can also lead to relevant signatures at high intensity fixed target experiments [105]. We save this work for future study.

In the presence of a black hole in the central regions of a galaxy the dark matter density may form a steep density spike. The density spike has important ramifications for indirect detection signals from dark matter annihilations studied here in this work. The change in the density spike scaling power law between CDM and SIDM models causes a significant

difference in the constraints for these models. We study Draco, the densest satellite dwarf galaxy of the Milky Way, and compute the indirect detection constraints for both CDM and SIDM. For a CDM model the predicted spike scales as $\rho \propto r^{-7/3}$ where as for SIDM the steepest expected power law is $\rho \propto r^{-7/4}$ which is more shallow. For black hole masses reasonable for the Draco system we find that the upper limit on the annihilation cross section is not sensitive for the SIDM model. In contrast, for the CDM model the possibility of an intermediate mass black hole has been excluded for a thermal relic.

We further study the constraints on the annihilation cross section for the Milky Way and the M87 galaxies. The annihilation signals coming from the supermassive black holes in these systems are significantly weakened in the SIDM model compared to CDM. Both the Milky Way and M87 exclude s wave annihilations from a thermal relic dark matter. However, a thermal relic scenario is still allowed for the SIDM model in these systems for larger dark matter masses. Furthermore, EHT observations of the M87 black hole can be a sensitive probe for the presence of an SIDM spike. In the future, the distribution of SIDM particles near a black hole could be studied which may play an important role in the strong gravitational limit in understanding the growth of supermassive black holes in the early Universe, see., e.g., [171, 172, 94].

Given the extreme densities inside of a NS, these compact objects make sensitive detectors for dark matter. Dark matter can be accelerated to relativistic speed by the steep gravitational well of a NS. Dark matter may then scatter off of the SM components present in the NS depositing kinetic energy heating up the NS to $\mathcal{O}(1000)$ K temperatures. SM processes predict that an old NS should cool to $\mathcal{O}(100)$ K temperatures so that there is an observable measurement that can be made to determine the presence of dark matter. In this work we study inelastic dark matter - electron scattering in a NS. The electrons are ultra-relativistic in this system and the calculation for the scattering requires a full relativistic treatment as in [185, 186]. Inelastic models of dark matter have the property that they

can evade terrestrial direct detection constraints for large enough mass splittings because the up-scattering becomes kinematically forbidden. However, because of the relativistic speeds of dark matter in-falling on a NS the mass gap is easily overcome.

We calculate the reach of NS heating for a dim-6 effective operation for fermionic dark matter. We also calculate the coupling reach for vector mediated dark matter in the kinetic mixing formalism. Finally, we study the pseudo-Dirac dark matter model presented in Chapter 2 kinetically mixed with the SM photon. We compare our results to the bounds from current and future collider and beam dump experiments taken from [175] for fixed ratio $m_\phi/m_\chi = 2$ and 3. We find that the NS bounds are superior to the terrestrial bounds by 2 to 3 orders of magnitude. Additionally, we show that NS bounds are sensitive to parameter space that neither current nor future terrestrial experiments can probe for inelastic SIDM. We explore a region in parameter space where the mass splitting is large enough to evade direct detection constraints ($\delta m = 1\ \mathrm{MeV}$) and can explain small scale structure. This study is exciting given that the observation of an $\mathcal{O}(10^9)$ yr aged NS at a temperature of $\mathcal{O}(1000)$ K temperature is experimentally viable for upcoming radio telescopes such as FAST [176], CHIME [177], SKA [178] and infrared telescopes like JWST [179],TMT [180], EELT [181]. A single observation of such a NS could be enough to discover dark matter or put strong constraints on dark matter models.

In light of the fact that dark matter is relegated to its gravitational effects on luminous matter and that to date there have been no direct detection signals from terrestrial experiments, it is very compelling to look toward astrophysical systems that could uncover the nature of dark matter. It has been hypothesized that dark matter may play a role in many of the open questions related to the SM of particle physics. For example, if dark matter carries a baryon number it could help to explain the apparent asymmetry between matter and antimatter [27, 199]. Dark matter may also play a role in the origin of the neutrino mass [200, 201]. Axion dark matter may be able to solve the strong CP problem [202, 203].

Understanding the particle nature of dark matter may resolve many of these issues. What we know for certain is that dark matter is central to understanding structure formation in the universe and that it makes up a large portion of the matter-energy budget of the cosmos. This work has shown that using the dynamics of dark matter halos, the annihilation signals coming from dense regions of dark matter near black holes and the kinetic heating of NS from dark matter - SM particle interactions are able to constrain models of dark matter. These astrophysical systems are complementary, and in some cases superior, to terrestrial experiments and can even probe dark matter models when it is not possible for terrestrial experiments. Astrophysical systems are an intriguing and in many cases very sensitive probe that should be utilized in the ultimate endeavor of uncovering the underlying nature of dark matter.

Appendices

APPENDIX A

INELASTIC DARK MATTER CROSS SECTION CALCULATIONS

A.1 Reformulation

In this appendix, we outline the variable phase space approach to reformulate equation (2.7); see [96] for a more detailed discussion on this method. The basic idea is to build a solution to equation (2.7) using solutions to the free-particle case ($\alpha_\chi \to 0$). In the non-interacting limit, the solutions can be written as superpositions of spherical Bessel and Neumann functions with constant coefficients. To build solutions to (2.7), we use superpositions of free-particle solutions and upgrade the coefficients to functions, i.e.,

$$\chi_i^{(l)}(x) = \alpha_i^{(l)}(x) f^{(l)}(p_i x) - \beta_i^{(l)}(x) g^{(l)}(p_i x), \tag{A.1}$$

where $\chi_i^{(l)}(x)$ are the component solutions to (2.7), $\alpha_i^{(l)}(x)$ and $\beta_i^{(l)}(x)$ are numerical functions, $p_i = a, c$, depending on the particle state, and $f^{(l)}(p_i x)$ and $g^{(l)}(p_i x)$ are the free-particle solutions. They obey the differential equation,

$$\left[\frac{d^2}{dx^2} - \frac{l(l+1)}{x^2} + p_i^2\right] z^{(l)}(p_i x) = 0. \tag{A.2}$$

where z takes the place of f or g. The function $f^{(l)}(p_i x)$ is defined to be regular at the origin and $g^{(l)}(p_i x)$ is irregular as $x \to 0$.

To form a general solution to equation (2.7), we must solve two coupled second-order differential equations. We therefore require four linearly independent solutions. The expression (A.1) represents only one of the four solutions but has four degrees of freedom; two of them come from $\alpha_i^{(l)}(x)$ and $\beta_i^{(l)}(x)$ and the other two from the normalization of

$f^{(l)}(p_i x)$ and $g^{(l)}(p_i x)$. We must impose constraints to reduce the extra degrees of freedom. Suppose that $d\chi_i^{(l)}(x)/dx$ is independent of the derivatives of $\alpha_i^{(l)}(x)$ and $\beta_i^{(l)}(x)$, which is trivially true for constant coefficients. This requires that

$$\frac{d\alpha_i^{(l)}(x)}{dx} f^{(l)}(p_i x) - \frac{d\beta_i^{(l)}(x)}{dx} g^{(l)}(p_i x) = 0. \tag{A.3}$$

We set the normalization of $f^{(l)}(p_i x)$ and $g^{(l)}(p_i x)$ by defining the Wronskian of the system to be

$$\frac{df^{(l)}(p_i x)}{d(p_i x)} g^{(l)}(p_i x) - f^{(l)}(p_i x) \frac{dg^{(l)}(p_i x)}{d(p_i x)} \equiv p_i. \tag{A.4}$$

After imposing the constraints, we have only one degree of freedom and an overall constant per linearly independent solution. A consistent choice for $f^{(l)}(p_i x)$ and $g^{(l)}(p_i x)$ is

$$f^{(l)}(p_i x) \equiv x j_l(p_i x),\ g^{(l)}(p_i x) \equiv i x h_l^{(1)}(p_i x), \tag{A.5}$$

where $j_l(p_i x)$ is the spherical Bessel function and $h_l^{(l)}(p_i x)$ is the spherical Hankel function of the first kind.

To keep track of the linearly independent solutions, we introduce a new subscript,

$$\chi_{in}(x) = \alpha_{in}(x) f(p_i x) - \beta_{in}(x) g(p_i x) \tag{A.6}$$

where we have dropped the angular momentum label l for brevity, $n = 1, 2$ for the two

independent solutions for a given $i = 1, 2$, which labels the particle state. Defining

$$\boldsymbol{f}(x) \equiv \begin{bmatrix} f(ax) & 0 \\ 0 & f(cx) \end{bmatrix},\ \boldsymbol{g}(x) \equiv \begin{bmatrix} g(ax) & 0 \\ 0 & g(cx) \end{bmatrix},\ \boldsymbol{\alpha}(x) \equiv \begin{bmatrix} \alpha_{11}(x) & \alpha_{12}(x) \\ \alpha_{21}(x) & \alpha_{22}(x) \end{bmatrix},$$
$$\boldsymbol{\beta}(x) \equiv \begin{bmatrix} \beta_{11}(x) & \beta_{12}(x) \\ \beta_{21}(x) & \beta_{22}(x) \end{bmatrix},\ \boldsymbol{\chi}(x) \equiv \begin{bmatrix} \chi_{11}(x) & \chi_{12}(x) \\ \chi_{21}(x) & \chi_{22}(x) \end{bmatrix} \tag{A.7}$$

we can rewrite equation (A.1) in a compact form,

$$\boldsymbol{\chi}(x) = \boldsymbol{f}(x)\boldsymbol{\alpha}(x) - \boldsymbol{g}(x)\boldsymbol{\beta}(x). \tag{A.8}$$

Further defining

$$\boldsymbol{\xi}(x) \equiv \boldsymbol{\chi}(x)\boldsymbol{\alpha}^{-1}(x),\ \boldsymbol{M}(x) \equiv \boldsymbol{\beta}(x)\boldsymbol{\alpha}^{-1}(x), \tag{A.9}$$

we have

$$\boldsymbol{\xi}(x) = \boldsymbol{f}(x) - \boldsymbol{g}(x)\boldsymbol{M}(x). \tag{A.10}$$

Taking the $x \to \infty$ limit of the choices for $f(p_i x)$ and $g(p_i x)$, we can see the virtue of the conventions and definitions employed so far,

$$\lim_{x\to\infty} f(p_i x) = \frac{(-i)^{l+1}e^{ip_i x} + (i)^{l+1}e^{-ip_i x}}{2},\ \lim_{x\to\infty} g(p_i x) = (-i)^{l+2}e^{ip_i x}. \tag{A.11}$$

Inserting (A.11) into (A.10) and comparing with equation (2.8), one can find that the components of $\boldsymbol{M}$ are related to the scattering amplitudes as

$$\frac{M_{11}(x\to\infty)}{a} = \alpha_x m_x \mathcal{F}_x,\quad \frac{M_{21}(x\to\infty)}{a} = \alpha_x m_x \mathcal{F}_y \tag{A.12}$$

where the incoming scatterers are of type 1. Similarly,

$$\frac{M_{12}(x \to \infty)}{c} = \alpha_x m_x \mathcal{F}_x, \quad \frac{M_{22}(x \to \infty)}{c} = \alpha_x m_x \mathcal{F}_y \tag{A.13}$$

for incoming particles of type 2. The i^{th} column of $\boldsymbol{\xi}$ is interpreted as the scattered wave functions for the two particle states where the incoming states are of type i. Next we make the definition,

$$U_{ij}(x) \equiv f(p_i x) g(p_i x) \delta_{ij} - g(p_j x) M_{ij}(x) g(p_j x). \tag{A.14}$$

Using the formalism developed in this subsection, we can derive the following first-order different equation for $U_{ij}(x)$,

$$\frac{dU_{ij}(x)}{dx} = p_i \delta_{ij} + \left(p_i \frac{g'(p_i x)}{g(p_i x)} + p_j \frac{g'(p_j x)}{g(p_j x)} \right) U_{ij}(x) - U_{il}(x) \frac{\tilde{V}_{lm}(x)}{p_l} U_{mj}(x) \tag{A.15}$$

where $\tilde{V}(x) \equiv \begin{bmatrix} 0 & -\frac{e^{-x/b}}{x} \\ -\frac{e^{-x/b}}{x} & 0 \end{bmatrix}$ and $g'(p_i x) \equiv dg(p_i x)/d(p_i x)$. As $x \to 0$, $\beta_{ij}(x) \to 0$ since the solution $\chi_{ij}(x)$ must be regular at the origin and we take $\alpha_{ij}(x) \to \delta_{ij}$. Therefore, $M_{ij}(x \to 0) = 0$ and the initial condition for $U_{ij}(x)$ becomes,

$$U_{ij}(x \to 0) = f(p_i x) g(p_i x) \delta_{ij}. \tag{A.16}$$

The advantage of this differential equation is that only logarithmic derivatives of the free solutions enter into the equation greatly increasing its numerical stability. We can now solve equation (A.15) using the initial condition (A.16) for $U_{ij}(x)$. Once $U_{ij}(x)$ is known then the scattering amplitudes $\sim M_{ij}(x)$ can be obtained using the definition (A.14). Finally, the scattering cross section can be calculated using equation (2.9). It is useful to note that the transformation $\delta m \to -\delta m$ changes the incoming particles from one type to the other

($a \leftrightarrow c$). Therefore we only need to solve for $M_{11}(x)$ and $M_{21}(x)$, once δm is changed to $-\delta m$, in order to obtain all scattering cross sections. Also, there is an equation for $\alpha_{ij}(x)$ ($\beta_{ij}(x)$) which carries information needed to solve for the Sommerfeld enhancements but are not needed in calculating the self-scattering cross sections [68].

A.2 Formulae

Here we develop formula for the total scattering cross section as well as the viscosity and transfer cross sections. Starting from equation (2.9), we can write the expression for the total cross section as

$$\sigma_{\rm tot} = \frac{p_{\rm out}}{p_{\rm in}} \sum_{l=0}^{\infty} \sum_{l'=0}^{\infty} (2l+1)(2l'+1) \mathcal{F}_l \mathcal{F}_{l'}^* \int d\Omega P_l(\cos\theta) P_{l'}^*(\cos\theta)). \tag{A.17}$$

Using the identity,

$$\int_{-1}^{1} dx P_l(x) P_{l'}^*(x) = \frac{2\delta_{ll'}}{(2l+1)} \tag{A.18}$$

the total cross section is given by

$$\sigma_{\rm tot} = 4\pi \frac{p_{\rm out}}{p_{\rm in}} \sum_{l=0}^{\infty} (2l+1) \left|\mathcal{F}_l\right|^2 . \tag{A.19}$$

The transfer cross section is weighted such that forward scattering events (scattering angle $\theta \to 0$) do not contribute at all and backward scattering events ($\theta \to \pi$) give the largest contribution to the cross section,

$$\sigma_T \equiv \frac{p_{\rm out}}{p_{\rm in}} \int d\Omega \left| \sum_{l=0}^{\infty} (2l+1) P_l(\cos\theta) \mathcal{F}_{\rm l} \right|^2 (1-\cos\theta). \tag{A.20}$$

Using (A.18) and the recursion relation

$$(l+1)P_{(l+1)}(x) = (2l+1)xP_l(x) - lP_{(l-1)}(x) \tag{A.21}$$

we have

$$\int_{-1}^{1} dx P_l(x) P^*_{l'}(x)(1-x) = \frac{2}{(2l+1)}\left[\delta_{ll'} - \frac{(l+1)}{(2l+3)}\delta_{(l+1)l'} - \frac{l}{(2l-1)}\delta_{(l-1)l'}\right]. \tag{A.22}$$

Identity (A.22) allows the transfer cross section to be written as,

$$\begin{aligned}\sigma_T &= 4\pi\frac{p_{\text{out}}}{p_{\text{in}}}\sum_{l=0}^{\infty}\left[(2l+1)\left|\mathcal{F}_l\right|^2 - (l+1)\mathcal{F}_l\mathcal{F}^*_{(l+1)} - l\mathcal{F}_l\mathcal{F}^*_{(l-1)}\right] \\ &= 4\pi\frac{p_{\text{out}}}{p_{\text{in}}}\sum_{l=0}^{\infty}\left[(2l+1)\left|\mathcal{F}_l\right|^2 - 2(l+1)Re(\mathcal{F}_l\mathcal{F}^*_{(l+1)})\right].\end{aligned} \tag{A.23}$$

We further write the scattering amplitude as a general complex number $\mathcal{F}_l \equiv |\mathcal{F}_l|\, e^{i\delta_l}$ and insert it into (A.23),

$$\sigma_T = 4\pi\frac{p_{\text{out}}}{p_{\text{in}}}\sum_{l=0}^{\infty}(l+1)\left[\left|\mathcal{F}_{(l+1)}\right|^2 + \left|\mathcal{F}_l\right|^2 - 2\left|\mathcal{F}_{(l+1)}\right|\left|\mathcal{F}_l\right|\cos(\delta_{(l+1)} - \delta_l)\right]. \tag{A.24}$$

Equation (A.24) has the benefit of being positive definite term-wise such that the sum is monotonically increasing. This property allows the sum to converge more quickly. The viscosity cross section is defined such that neither forward nor backward scattering contribute to the cross section,

$$\sigma_V \equiv \frac{p_{\text{out}}}{p_{\text{in}}}\int d\Omega \left|\sum_{l=0}^{\infty}(2l+1)P_l(\cos\theta)\mathcal{F}_l\right|^2 \sin^2\theta. \tag{A.25}$$

Following a similar procedure to the transfer cross section calculation and using identities (A.18) and (A.21), we can derive the following identity

$$\int_{-1}^{1} dx P_l(x) P_{l'}^*(x)(1-x^2) = \frac{2}{(2l+1)}\Bigg[\left(1 - \frac{(l+1)^2}{(2l+1)(2l+3)} - \frac{l^2}{(2l+1)(2l-1)}\right)\delta_{ll'} - \frac{(l+1)(l+2)}{(2l+3)(2l+5)}\delta_{(l+2)l'} - \frac{l(l-1)}{(2l-1)(2l-3)}\delta_{(l-2)l'}\Bigg]. \tag{A.26}$$

The viscosity cross section is then,

$$\begin{aligned}\sigma_V &= 4\pi\frac{p_{\text{out}}}{p_{\text{in}}}\sum_{l=0}^{\infty}\Bigg[\left((2l+1) - \frac{(l+1)^2}{(2l+3)} - \frac{l^2}{(2l-1)}\right)|\mathcal{F}_l|^2 \\ &\qquad - \frac{(l+1)(l+2)}{(2l+3)}\mathcal{F}_l\mathcal{F}_{(l+2)}^* - \frac{l(l-1)}{(2l-1)}\mathcal{F}_l\mathcal{F}_{(l-2)}^*\Bigg] \qquad \text{(A.27)} \\ &= 4\pi\frac{p_{\text{out}}}{p_{\text{in}}}\sum_{l=0}^{\infty}\left[\frac{2(2l+1)(l^2+l-1)}{(2l+3)(2l-1)}|\mathcal{F}_l|^2 - \frac{2(l+2)(l+1)}{(2l+3)}Re(\mathcal{F}_l\mathcal{F}_{(l+2)}^*)\right].\end{aligned}$$

Rewriting $\mathcal{F}_l$ in polar form gives the final result,

$$\sigma_V = 4\pi\frac{p_{\text{out}}}{p_{\text{in}}}\sum_{l=0}^{\infty}\frac{(l+1)(l+2)}{(2l+3)}\left[\left|\mathcal{F}_{(l+2)}\right|^2 + |\mathcal{F}_l|^2 - 2\left|\mathcal{F}_{(l+2)}\right||\mathcal{F}_l|\cos(\delta_{(l+2)} - \delta_l)\right] \tag{A.28}$$

which is again term-wise positive definite.

APPENDIX B

RECOIL RATES AND TERRESTRIAL DIRECT DETECTION

In this model, dark matter couples to the visible sector particles via the mixing of the dark photon with the U(1) hypercharge gauge boson. In the mass bases, the diagonalized lagrangian is

$$\begin{aligned}\mathcal{L} =&\frac{1}{2}\bar{\chi_1}(i\partial\!\!\!/ - m_1)\chi_1 + \frac{1}{2}\bar{\chi_2}(i\partial\!\!\!/ - m_2)\chi_2 - \frac{1}{4}F'_{\mu\nu}F'^{\mu\nu} + \frac{1}{2}m_\phi^2\Phi'_\mu\Phi'^\mu \\ &- \left(\frac{1}{2}g_\chi\bar{\chi_2}\gamma^\mu\chi_1\Phi_\mu + h.c.\right) + q\epsilon\bar{\psi}\gamma^\mu\psi\Phi_\mu\end{aligned} \tag{B.1}$$

where χ_1 and χ_2 are two species of dark matter with a mass difference of $\delta m = m_2 - m_1$. The dark photon Φ is a massive U(1) gauge boson with mass m_ϕ and can be either a scalar or a vector mediator. Here we take Φ to be a vector with a field strength $F'_{\mu\nu} = (\partial_\mu\Phi_\nu - \partial_\nu\Phi_\mu)$ and a kinetic mixing term with coupling ϵ.

In ground-based detectors, dark matter particles scatter off nuclei and the scattering rate for a given recoil energy $E_{\rm R}$ is

$$\frac{dR}{dE_{\rm R}} = \left\langle n_\chi v\frac{d\sigma}{dE_{\rm R}}\right\rangle = n_{\rm T}\frac{\rho_\chi}{m_\chi}\int_{v_{\rm min}}^{v_{\rm max}} v f_e(v)\frac{d\sigma}{dE_{\rm R}}d^3v \tag{B.2}$$

where $n_{\rm T}$ is the number of target nuclei per unit mass of the detector, $n_\chi = \rho_\chi/m_\chi$ is the local number density using $\rho_\chi \approx 0.3\ {\rm GeV/cm^3}$, $f_e(v)$ is the dark matter velocity distribution function in the galactic halo and $d\sigma/dE_{\rm R}$ is the differential cross-section for scattering between dark matter and the nucleus.

Since the detectors are Earth based, all the equations are written in the Earth's reference

frame. The velocity of the Earth in the Milky Way is given by

$$v_e = v_\odot + v_{\rm orb}\cos\gamma\cos(\omega(t-t_0)) \tag{B.3}$$

where $v_\odot = v_0 + 12\ \mathrm{km/s}$ is the speed of the Sun in the rest frame of the galaxy, $v_0 = 220\ \mathrm{km/s}$ is the rotational speed of the local standard of rest, $\cos\gamma = 0.51$ is the angle between the solar plane and the galactic plane, $v_{\rm orb} = 30\ \mathrm{km/s}$ is the speed of the Earth in the solar system, $\omega = 2\pi/365\ \mathrm{rad/day}$ is the period of rotation of the Earth around the Sun and $t_0 = 152$ (June 2nd) corresponds to the day with the maximum speed of the Earth. For the dark matter velocity distribution function in the reference frame of the Earth we use a truncated Maxwell-Boltzmann distribution,

$$f_e(v) = Ne^{-\frac{(v-v_e)^2}{v_0^2}}\Theta(v - v_{\rm max}) \tag{B.4}$$

where $N = 1/\left(\pi^{3/2}v_0^3\mathrm{Erf}(v_{\rm esc}/v_0) - 2v_{\rm esc}\exp(-v_{\rm esc}^2/v_0^2)\right)$ is a normalization factor, $\Theta(v - v_{\rm max})$ is a Heaviside step function, $v_{\rm esc} = 533\ \mathrm{km/s}$ is the escape velocity of dark matter in the halo and $v_{\rm max} = v_e + v_{\rm esc}$ is the maximum velocity of incoming dark matter in the detector. On the other hand, the minimum velocity of dark matter required for scattering to occur at a given recoil energy $E_{\rm R}$ and mass $m_{\rm N}$ of the nucleus is $v_{\rm min} \approx (E_{\rm R}m_{\rm N}/(\mu + \delta m))/\sqrt{2E_{\rm R}m_{\rm N}}$ where μ is the reduced mass of m_1 and $m_{\rm N}$. The velocity integral in Eq. B.2 depends on the relative magnitude of $v_{\rm min}$ and $|v_{\rm esc} - v_e|$,

$$\int_{v_{\rm min}}^{v_{\rm max}} d^3v = 2\pi \begin{cases} \displaystyle\int_{v_{\rm min}}^{v_{\rm esc}-v_e} v^2dv \int_{-1}^{1} d(\cos(\theta)) + \int_{v_{\rm esc}-v_e}^{v_{\rm esc}+v_e} v^2dv \int_{-1}^{c^*} d(\cos(\theta)), & v_{\rm min} < v_{\rm esc} - v_e \\ \displaystyle\int_{v_{\rm min}}^{v_{\rm esc}+v_e} v^2dv \int_{-1}^{c^*} d(\cos(\theta)), & v_{\rm esc} - v_e < v_{\rm min} < v_{\rm esc} + v_e \end{cases} \tag{B.5}$$

where $c^* = (v_{\rm esc}^2 - v^2 - v_e^2/(2vv_e))$ gives the minimum angle consistent with scattering for a given recoil energy when $v_{\rm esc} - v_e < v_{\rm min} < v_{\rm esc} + v_e$.

The scattering differential cross-section in the non-relativistic limit is

$$\frac{d\sigma}{dE_{\rm R}} \approx \frac{m_{\rm N}}{2v^2} \frac{16\pi\alpha_\chi\alpha_{\rm em}\epsilon^2 Z^2}{(m_\phi^2 - \delta m^2 + 2m_{\rm N}E_{\rm R})^2} F(E_{\rm R})^2 \tag{B.6}$$

where $\alpha_{\rm em}$ and α_χ are the visible and dark sector fine structure constants respectively, Z is the atomic number of the detector nucleus and F^2 is the nuclear form factor. Here we use a form factor specific for Xenon [193, 204],

$$F(E_{\rm R})^2 = \frac{e^{-u}}{A^2}\left(A + \sum_{n=1}^{5} c_n u^n\right) \tag{B.7}$$

where $u = q^2b^2/2$, $b^2 = m_n^{-1}(45A^{-1/2} - 25A^{-2/3})^{-1}\ {\rm MeV}^{-1}$, $q^2 = 2m_{\rm N}E_{\rm R}$, m_n is the mass of the neutron, A is the mass number of the Xenon and the coefficients c_n for the Xe_{54}^{132} isotope are as follows [204],

$$\begin{cases} c_1 = -132.841 \\ c_2 = 38.4859 \\ c_3 = -4.08455 \\ c_4 = 0.153298 \\ c_5 = -0.0013897 \end{cases} \tag{B.8}$$

Finally, we integrate Eq. B.2 on the energy threshold of the detector and calculate upper bounds on the parameter space by setting the calculated number of events to the observed number of events. Specifically, for the Xenon1T experiment the thresholds are $4.9 - 40.9\ {\rm keV}$ for the nuclear recoil and $1.4 - 10.6\ {\rm keV}$ for the electron recoil [205]. In

the $1.3 \times 278.8\ \mathrm{ton\ day}$ exposure of liquid Xe^{132}_{54} no significant excessive events over background were observed. At the 90% confidence level, zero observed events is equivalent to 2.8 total events.

REFERENCES

[1] P. W. Higgs, "Broken Symmetries and the Masses of Gauge Bosons," *Phys. Rev. Lett.*, vol. 13, J. C. Taylor, Ed., pp. 508–509, 1964.

[2] F. Englert and R. Brout, "Broken Symmetry and the Mass of Gauge Vector Mesons," *Phys. Rev. Lett.*, vol. 13, J. C. Taylor, Ed., pp. 321–323, 1964.

[3] C.-N. Yang and R. L. Mills, "Conservation of Isotopic Spin and Isotopic Gauge Invariance," *Phys. Rev.*, vol. 96, J.-P. Hsu and D. Fine, Eds., pp. 191–195, 1954.

[4] S. Weinberg, "A Model of Leptons," *Phys. Rev. Lett.*, vol. 19, pp. 1264–1266, 1967.

[5] A. Salam, "Weak and Electromagnetic Interactions," *Conf. Proc. C*, vol. 680519, pp. 367–377, 1968.

[6] S. L. Glashow, "Partial Symmetries of Weak Interactions," *Nucl. Phys.*, vol. 22, pp. 579–588, 1961.

[7] M. Gell-Mann, "The Eightfold Way: A Theory of strong interaction symmetry," Mar. 1961.

[8] T. P. Cheng and L. F. Li, *GAUGE THEORY OF ELEMENTARY PARTICLE PHYSICS*. 1984, ISBN: 978-0-19-851961-4.

[9] M. Kobayashi and T. Maskawa, "CP Violation in the Renormalizable Theory of Weak Interaction," *Prog. Theor. Phys.*, vol. 49, pp. 652–657, 1973.

[10] N. Cabibbo, "Unitary Symmetry and Leptonic Decays," *Phys. Rev. Lett.*, vol. 10, pp. 531–533, 1963.

[11] D. J. Gross and F. Wilczek, "Ultraviolet Behavior of Nonabelian Gauge Theories," *Phys. Rev. Lett.*, vol. 30, J. C. Taylor, Ed., pp. 1343–1346, 1973.

[12] H. D. Politzer, "Reliable Perturbative Results for Strong Interactions?" *Phys. Rev. Lett.*, vol. 30, J. C. Taylor, Ed., pp. 1346–1349, 1973.

[13] L. Di Lella and C. Rubbia, "The Discovery of the W and Z Particles," *Adv. Ser. Direct. High Energy Phys.*, vol. 23, pp. 137–163, 2015.

[14] J. Ellis, "The Discovery of the Gluon," *Int. J. Mod. Phys. A*, vol. 29, no. 31, H. Fritzsch and M. Gell-Mann, Eds., p. 1 430 072, 2014. arXiv: 1409.4232 [hep-ph].

[15] C. Campagnari and M. Franklin, "The Discovery of the top quark," *Rev. Mod. Phys.*, vol. 69, pp. 137–212, 1997. arXiv: hep-ex/9608003.

[16] J. J. Aubert *et al.*, "Experimental Observation of a Heavy Particle J," *Phys. Rev. Lett.*, vol. 33, pp. 1404–1406, 1974.

[17] G. Aad *et al.*, "Observation of a new particle in the search for the Standard Model Higgs boson with the ATLAS detector at the LHC," *Phys. Lett. B*, vol. 716, pp. 1–29, 2012. arXiv: 1207.7214 [hep-ex].

[18] D. Hanneke, S. Fogwell, and G. Gabrielse, "New Measurement of the Electron Magnetic Moment and the Fine Structure Constant," *Phys. Rev. Lett.*, vol. 100, p. 120 801, 2008. arXiv: 0801.1134 [physics.atom-ph].

[19] G. Altarelli and M. W. Grunewald, "Precision electroweak tests of the standard model," *Phys. Rept.*, vol. 403-404, pp. 189–201, 2004. arXiv: hep-ph/0404165.

[20] Q. R. Ahmad *et al.*, "Direct evidence for neutrino flavor transformation from neutral current interactions in the Sudbury Neutrino Observatory," *Phys. Rev. Lett.*, vol. 89, p. 011 301, 2002. arXiv: nucl-ex/0204008.

[21] Y. Fukuda *et al.*, "Evidence for oscillation of atmospheric neutrinos," *Phys. Rev. Lett.*, vol. 81, pp. 1562–1567, 1998. arXiv: hep-ex/9807003.

[22] K. M. Heeger, "Evidence for neutrino mass: A Decade of discovery," in *SEESAW25: International Conference on the Seesaw Mechanism and the Neutrino Mass*, Dec. 2004, pp. 65–80. arXiv: hep-ex/0412032.

[23] H.-Y. Cheng, "The Strong CP Problem Revisited," *Phys. Rept.*, vol. 158, p. 1, 1988.

[24] T. Mannel, "Theory and phenomenology of CP violation," *Nucl. Phys. B Proc. Suppl.*, vol. 167, G. Borisov, M. Bozzo, R. Jones, C. S. Kalman, P. Ratoff, M. Smizanska, and N. Solomey, Eds., pp. 115–119, 2007.

[25] L. Canetti, M. Drewes, and M. Shaposhnikov, "Matter and Antimatter in the Universe," *New J. Phys.*, vol. 14, p. 095 012, 2012. arXiv: 1204.4186 [hep-ph].

[26] A. D. Sakharov, "Violation of CP Invariance, C asymmetry, and baryon asymmetry of the universe," *Pisma Zh. Eksp. Teor. Fiz.*, vol. 5, pp. 32–35, 1967.

[27] Y. Cui and M. Shamma, "WIMP Cogenesis for Asymmetric Dark Matter and the Baryon Asymmetry," *JHEP*, vol. 12, p. 046, 2020. arXiv: 2002.05170 [hep-ph].

[28] P. J. E. Peebles and B. Ratra, "The Cosmological Constant and Dark Energy," *Rev. Mod. Phys.*, vol. 75, J.-P. Hsu and D. Fine, Eds., pp. 559–606, 2003. arXiv: astro-ph/0207347.

[29] S. M. Carroll, "The Cosmological constant," *Living Rev. Rel.*, vol. 4, p. 1, 2001. arXiv: astro-ph/0004075.

[30] F. Zwicky, "Die Rotverschiebung von extragalaktischen Nebeln," *Helv. Phys. Acta*, vol. 6, pp. 110–127, 1933.

[31] G. Bertone and D. Hooper, "History of dark matter," *Rev. Mod. Phys.*, vol. 90, no. 4, p. 045 002, 2018. arXiv: 1605.04909 [astro-ph.CO].

[32] Y. Sofue and V. Rubin, "Rotation curves of spiral galaxies," *Ann. Rev. Astron. Astrophys.*, vol. 39, pp. 137–174, 2001. arXiv: astro-ph/0010594.

[33] A. V. Zasov, A. S. Saburova, A. V. Khoperskov, and S. A. Khoperskov, "Dark matter in galaxies," *Phys. Usp.*, vol. 60, no. 1, pp. 3–39, 2017. arXiv: 1710.10630 [astro-ph.GA].

[34] A. Robertson, R. Massey, and V. Eke, "What does the Bullet Cluster tell us about self-interacting dark matter?" *Mon. Not. Roy. Astron. Soc.*, vol. 465, no. 1, pp. 569–587, 2017. arXiv: 1605.04307 [astro-ph.CO].

[35] M. Markevitch, A. H. Gonzalez, D. Clowe, A. Vikhlinin, L. David, W. Forman, C. Jones, S. Murray, and W. Tucker, "Direct constraints on the dark matter self-interaction cross-section from the merging galaxy cluster 1E0657-56," *Astrophys. J.*, vol. 606, pp. 819–824, 2004. arXiv: astro-ph/0309303.

[36] K. Freese, "Status of Dark Matter in the Universe," *Int. J. Mod. Phys.*, vol. 1, no. 06, M. Bianchi, R. T. Jantzen, and R. Ruffini, Eds., pp. 325–355, 2017. arXiv: 1701.01840 [astro-ph.CO].

[37] C. L. Bennett *et al.*, "Nine-Year Wilkinson Microwave Anisotropy Probe (WMAP) Observations: Final Maps and Results," *Astrophys. J. Suppl.*, vol. 208, p. 20, 2013. arXiv: 1212.5225 [astro-ph.CO].

[38] J. R. Primack, "Dark matter and structure formation," in *Midrasha Mathematicae in Jerusalem: Winter School in Dynamical Systems*, Jul. 1997. arXiv: astro-ph/9707285.

[39] R. H. Wechsler and J. L. Tinker, "The Connection between Galaxies and their Dark Matter Halos," *Ann. Rev. Astron. Astrophys.*, vol. 56, pp. 435–487, 2018. arXiv: 1804.03097 [astro-ph.GA].

[40] C. Alcock *et al.*, "The MACHO project: Microlensing results from 5.7 years of LMC observations," *Astrophys. J.*, vol. 542, pp. 281–307, 2000. arXiv: astro-ph/0001272.

[41] S. Profumo, L. Giani, and O. F. Piattella, "An Introduction to Particle Dark Matter," *Universe*, vol. 5, no. 10, p. 213, 2019. arXiv: 1910.05610 [hep-ph].

[42] G. Bertone, D. Hooper, and J. Silk, "Particle dark matter: Evidence, candidates and constraints," *Phys. Rept.*, vol. 405, pp. 279–390, 2005. arXiv: hep-ph/0404175.

[43] S. D. McDermott, H.-B. Yu, and K. M. Zurek, "Turning off the Lights: How Dark is Dark Matter?" *Phys. Rev. D*, vol. 83, p. 063 509, 2011. arXiv: 1011.2907 [hep-ph].

[44] N. Aghanim *et al.*, "Planck 2018 results. VI. Cosmological parameters," *Astron. Astrophys.*, vol. 641, A6, 2020, [Erratum: Astron.Astrophys. 652, C4 (2021)]. arXiv: 1807.06209 [astro-ph.CO].

[45] A. Arbey and F. Mahmoudi, "Dark matter and the early Universe: a review," *Prog. Part. Nucl. Phys.*, vol. 119, p. 103 865, 2021. arXiv: 2104.11488 [hep-ph].

[46] S. Hannestad, A. Mirizzi, G. G. Raffelt, and Y. Y. Y. Wong, "Neutrino and axion hot dark matter bounds after WMAP-7," *JCAP*, vol. 08, p. 001, 2010. arXiv: 1004.0695 [astro-ph.CO].

[47] A. Boyarsky, M. Drewes, T. Lasserre, S. Mertens, and O. Ruchayskiy, "Sterile neutrino Dark Matter," *Prog. Part. Nucl. Phys.*, vol. 104, pp. 1–45, 2019. arXiv: 1807.07938 [hep-ph].

[48] J. Brandbyge and S. Hannestad, "Cosmological N-body simulations with generic hot dark matter," *JCAP*, vol. 10, p. 015, 2017. arXiv: 1706.00025 [astro-ph.CO].

[49] J. S. Bullock and M. Boylan-Kolchin, "Small-Scale Challenges to the ΛCDM Paradigm," *Ann. Rev. Astron. Astrophys.*, vol. 55, pp. 343–387, 2017. arXiv: 1707.04256 [astro-ph.CO].

[50] J. R. Primack, "Cosmology: small scale issues," *AIP Conf. Proc.*, vol. 1166, no. 1, D. B. Cline, Ed., pp. 3–9, 2009. arXiv: 0902.2506 [astro-ph.CO].

[51] A. Del Popolo and M. Le Delliou, "Small scale problems of the ΛCDM model: a short review," *Galaxies*, vol. 5, no. 1, p. 17, 2017. arXiv: 1606.07790 [astro-ph.CO].

[52] D. N. Spergel and P. J. Steinhardt, "Observational evidence for selfinteracting cold dark matter," *Phys. Rev. Lett.*, vol. 84, pp. 3760–3763, 2000. arXiv: astro-ph/9909386 [astro-ph].

[53] S. Tulin and H.-B. Yu, "Dark Matter Self-interactions and Small Scale Structure," *Phys. Rept.*, vol. 730, pp. 1–57, 2018. arXiv: 1705.02358 [hep-ph].

[54] A. Kamada, M. Kaplinghat, A. B. Pace, and H.-B. Yu, "How the Self-Interacting Dark Matter Model Explains the Diverse Galactic Rotation Curves," *Phys. Rev. Lett.*, vol. 119, no. 11, p. 111 102, 2017. arXiv: 1611.02716 [astro-ph.GA].

[55] P. Creasey, O. Sameie, L. V. Sales, H.-B. Yu, M. Vogelsberger, and J. Zavala, "Spreading out and staying sharp – creating diverse rotation curves via baryonic and self-interaction effects," *Mon. Not. Roy. Astron. Soc.*, vol. 468, no. 2, pp. 2283–2295, 2017. arXiv: 1612.03903 [astro-ph.GA].

[56] O. Sameie, A. J. Benson, L. V. Sales, H.-B. Yu, L. A. Moustakas, and P. Creasey, "The Effect of Dark Matter–Dark Radiation Interactions on Halo Abundance: A Press–Schechter Approach," *Astrophys. J.*, vol. 874, no. 1, p. 101, 2019. arXiv: 1810.11040 [astro-ph.CO].

[57] M. Rocha, A. H. G. Peter, J. S. Bullock, M. Kaplinghat, S. Garrison-Kimmel, J. Onorbe, and L. A. Moustakas, "Cosmological Simulations with Self-Interacting Dark Matter I: Constant Density Cores and Substructure," *Mon. Not. Roy. Astron. Soc.*, vol. 430, pp. 81–104, 2013. arXiv: 1208.3025 [astro-ph.CO].

[58] S. Tulin, H.-B. Yu, and K. M. Zurek, "Beyond Collisionless Dark Matter: Particle Physics Dynamics for Dark Matter Halo Structure," *Phys. Rev. D*, vol. 87, no. 11, p. 115 007, 2013. arXiv: 1302.3898 [hep-ph].

[59] G. Alvarez and H.-B. Yu, "Astrophysical probes of inelastic dark matter with a light mediator," *Phys. Rev. D*, vol. 101, no. 4, p. 043 002, 2020. arXiv: 1911.11114 [hep-ph].

[60] G. Alvarez and H.-B. Yu, "Density spikes near black holes in self-interacting dark matter halos and indirect detection constraints," *Phys. Rev. D*, vol. 104, no. 4, p. 043 013, 2021. arXiv: 2012.15050 [hep-ph].

[61] G. Alvarez, A. Joglekar, M. P. Mehrdad, and H.-B. Yu, "Heating of Neutron Stars with Relativistic Targets by Inelastic Dark Matter," 2021 [Upcoming].

[62] M. Kaplinghat, S. Tulin, and H.-B. Yu, "Direct Detection Portals for Self-interacting Dark Matter," *Phys. Rev.*, vol. D89, no. 3, p. 035 009, 2014. arXiv: 1310.7945 [hep-ph].

[63] E. Del Nobile, M. Kaplinghat, and H.-B. Yu, "Direct Detection Signatures of Self-Interacting Dark Matter with a Light Mediator," *JCAP*, vol. 1510, no. 10, p. 055, 2015. arXiv: 1507.04007 [hep-ph].

[64] X. Ren *et al.*, "Constraining Dark Matter Models with a Light Mediator at the PandaX-II Experiment," *Phys. Rev. Lett.*, vol. 121, no. 2, p. 021 304, 2018. arXiv: 1802.06912 [hep-ph].

[65] D. S. Akerib *et al.*, "Results of a Search for Sub-GeV Dark Matter Using 2013 LUX Data," *Phys. Rev. Lett.*, vol. 122, no. 13, p. 131 301, 2019. arXiv: 1811.11241 [astro-ph.CO].

[66] E. Aprile *et al.*, "Light Dark Matter Search with Ionization Signals in XENON1T," 2019. arXiv: 1907.11485 [hep-ex].

[67] Y. Zhang, "Self-interacting Dark Matter Without Direct Detection Constraints," *Phys. Dark Univ.*, vol. 15, pp. 82–89, 2017. arXiv: 1611.03492 [hep-ph].

[68] M. Blennow, S. Clementz, and J. Herrero-Garcia, "Self-interacting inelastic dark matter: A viable solution to the small scale structure problems," *JCAP*, vol. 1703, no. 03, p. 048, 2017. arXiv: 1612.06681 [hep-ph].

[69] T. Han and R. Hempfling, "Messenger sneutrinos as cold dark matter," *Phys. Lett.*, vol. B415, pp. 161–169, 1997. arXiv: hep-ph/9708264 [hep-ph].

[70] D. Tucker-Smith and N. Weiner, "Inelastic dark matter," *Phys. Rev.*, vol. D64, p. 043 502, 2001. arXiv: hep-ph/0101138 [hep-ph].

[71] K. Schutz and T. R. Slatyer, "Self-Scattering for Dark Matter with an Excited State," *JCAP*, vol. 1501, no. 01, p. 021, 2015. arXiv: 1409.2867 [hep-ph].

[72] D. P. Finkbeiner and N. Weiner, "Exciting Dark Matter and the INTEGRAL/SPI 511 keV signal," *Phys. Rev.*, vol. D76, p. 083 519, 2007. arXiv: astro-ph/0702587 [astro-ph].

[73] N. Arkani-Hamed, D. P. Finkbeiner, T. R. Slatyer, and N. Weiner, "A Theory of Dark Matter," *Phys. Rev. D*, vol. 79, p. 015 014, 2009. arXiv: 0810.0713 [hep-ph].

[74] A. Loeb and N. Weiner, "Cores in Dwarf Galaxies from Dark Matter with a Yukawa Potential," *Phys. Rev. Lett.*, vol. 106, p. 171 302, 2011. arXiv: 1011.6374 [astro-ph.CO].

[75] D. P. Finkbeiner and N. Weiner, "X-ray line from exciting dark matter," *Phys. Rev.*, vol. D94, no. 8, p. 083 002, 2016. arXiv: 1402.6671 [hep-ph].

[76] R. N. Mohapatra and V. L. Teplitz, "Mirror dark matter and galaxy core densities of galaxies," *Phys. Rev.*, vol. D62, p. 063 506, 2000. arXiv: astro-ph/0001362 [astro-ph].

[77] R. N. Mohapatra, S. Nussinov, and V. L. Teplitz, "Mirror matter as selfinteracting dark matter," *Phys. Rev.*, vol. D66, p. 063 002, 2002. arXiv: hep-ph/0111381 [hep-ph].

[78] D. E. Kaplan, G. Z. Krnjaic, K. R. Rehermann, and C. M. Wells, "Atomic Dark Matter," *JCAP*, vol. 1005, p. 021, 2010. arXiv: 0909.0753 [hep-ph].

[79] M. Yu. Khlopov, A. G. Mayorov, and E. Yu. Soldatov, "The dark atoms of dark matter," *Prespace. J.*, vol. 1, pp. 1403–1417, 2010. arXiv: 1012.0934 [astro-ph.CO].

[80] J. M. Cline, Z. Liu, and W. Xue, "Millicharged Atomic Dark Matter," *Phys. Rev.*, vol. D85, p. 101 302, 2012. arXiv: 1201.4858 [hep-ph].

[81] F.-Y. Cyr-Racine and K. Sigurdson, "Cosmology of atomic dark matter," *Phys. Rev.*, vol. D87, no. 10, p. 103 515, 2013. arXiv: 1209.5752 [astro-ph.CO].

[82] J. M. Cline, Z. Liu, G. Moore, and W. Xue, "Scattering properties of dark atoms and molecules," *Phys. Rev.*, vol. D89, no. 4, p. 043 514, 2014. arXiv: 1311.6468 [hep-ph].

[83] R. Foot, "Mirror dark matter: Cosmology, galaxy structure and direct detection," *Int. J. Mod. Phys.*, vol. A29, p. 1 430 013, 2014. arXiv: 1401.3965 [astro-ph.CO].

[84] R. Foot and S. Vagnozzi, "Dissipative hidden sector dark matter," *Phys. Rev.*, vol. D91, p. 023 512, 2015. arXiv: 1409.7174 [hep-ph].

[85] K. K. Boddy, M. Kaplinghat, A. Kwa, and A. H. G. Peter, "Hidden Sector Hydrogen as Dark Matter: Small-scale Structure Formation Predictions and the Importance of Hyperfine Interactions," *Phys. Rev.*, vol. D94, no. 12, p. 123 017, 2016. arXiv: 1609.03592 [hep-ph].

[86] M. R. Buckley and A. DiFranzo, "Collapsed Dark Matter Structures," *Phys. Rev. Lett.*, vol. 120, no. 5, p. 051 102, 2018. arXiv: 1707.03829 [hep-ph].

[87] M. T. Frandsen and S. Sarkar, "Asymmetric dark matter and the Sun," *Phys. Rev. Lett.*, vol. 105, p. 011 301, 2010. arXiv: 1003.4505 [hep-ph].

[88] M. T. Frandsen, S. Sarkar, and K. Schmidt-Hoberg, "Light asymmetric dark matter from new strong dynamics," *Phys. Rev.*, vol. D84, p. 051 703, 2011. arXiv: 1103.4350 [hep-ph].

[89] K. K. Boddy, J. L. Feng, M. Kaplinghat, Y. Shadmi, and T. M. P. Tait, "Strongly interacting dark matter: Self-interactions and keV lines," *Phys. Rev.*, vol. D90, no. 9, p. 095 016, 2014. arXiv: 1408.6532 [hep-ph].

[90] E. Braaten, D. Kang, and R. Laha, "Production of dark-matter bound states in the early universe by three-body recombination," *JHEP*, vol. 11, p. 084, 2018. arXiv: 1806.00609 [hep-ph].

[91] J. L. Feng, M. Kaplinghat, and H.-B. Yu, "Halo Shape and Relic Density Exclusions of Sommerfeld-Enhanced Dark Matter Explanations of Cosmic Ray

Excesses," *Phys. Rev. Lett.*, vol. 104, p. 151 301, 2010. arXiv: 0911.0422 [hep-ph].

[92] A. Das and B. Dasgupta, "New dissipation mechanisms from multilevel dark matter scattering," *Phys. Rev.*, vol. D97, no. 2, p. 023 002, 2018. arXiv: 1709.06577 [hep-ph].

[93] R. Essig, S. D. Mcdermott, H.-B. Yu, and Y.-M. Zhong, "Constraining Dissipative Dark Matter Self-Interactions," *Phys. Rev. Lett.*, vol. 123, no. 12, p. 121 102, 2019. arXiv: 1809.01144 [hep-ph].

[94] J. Choquette, J. M. Cline, and J. M. Cornell, "Early formation of supermassive black holes via dark matter self-interactions," *JCAP*, vol. 07, p. 036, 2019. arXiv: 1812.05088 [astro-ph.CO].

[95] B. Batell, M. Pospelov, and A. Ritz, "Direct Detection of Multi-component Secluded WIMPs," *Phys. Rev.*, vol. D79, p. 115 019, 2009. arXiv: 0903.3396 [hep-ph].

[96] S. N. Ershov, J. S. Vaagen, and M. V. Zhukov, "Modified variable phase method for the solution of coupled radial Schrodinger equations," *Phys. Rev.*, vol. C84, p. 064 308, 2011.

[97] C. Boehm and P. Fayet, "Scalar dark matter candidates," *Nucl. Phys.*, vol. B683, pp. 219–263, 2004. arXiv: hep-ph/0305261 [hep-ph].

[98] M. Pospelov, A. Ritz, and M. B. Voloshin, "Secluded WIMP Dark Matter," *Phys. Lett.*, vol. B662, pp. 53–61, 2008. arXiv: 0711.4866 [hep-ph].

[99] J. L. Feng and J. Kumar, "The WIMPless Miracle: Dark-Matter Particles without Weak-Scale Masses or Weak Interactions," *Phys. Rev. Lett.*, vol. 101, p. 231 301, 2008. arXiv: 0803.4196 [hep-ph].

[100] J. L. Feng, H. Tu, and H.-B. Yu, "Thermal Relics in Hidden Sectors," *JCAP*, vol. 0810, p. 043, 2008. arXiv: 0808.2318 [hep-ph].

[101] S. Tulin, H.-B. Yu, and K. M. Zurek, "Resonant Dark Forces and Small Scale Structure," *Phys. Rev. Lett.*, vol. 110, no. 11, p. 111 301, 2013. arXiv: 1210.0900 [hep-ph].

[102] A. B. Newman, T. Treu, R. S. Ellis, and D. J. Sand, "The Density Profiles of Massive, Relaxed Galaxy Clusters: II. Separating Luminous and Dark Matter in

Cluster Cores," *Astrophys. J.*, vol. 765, p. 25, 2013. arXiv: 1209.1392 [astro-ph.CO].

[103] M. Kaplinghat, S. Tulin, and H.-B. Yu, "Dark Matter Halos as Particle Colliders: Unified Solution to Small-Scale Structure Puzzles from Dwarfs to Clusters," *Phys. Rev. Lett.*, vol. 116, no. 4, p. 041 302, 2016. arXiv: 1508.03339 [astro-ph.CO].

[104] Y. Tsai, T. Xu, and H.-B. Yu, "Displaced Lepton Jet Signatures from Self-Interacting Dark Matter Bound States," *JHEP*, vol. 08, p. 131, 2019. arXiv: 1811.05999 [hep-ph].

[105] Y.-D. Tsai, P. deNiverville, and M. X. Liu, "The High-Energy Frontier of the Intensity Frontier: Closing the Dark Photon, Inelastic Dark Matter, and Muon g-2 Windows," 2019. arXiv: 1908.07525 [hep-ph].

[106] J. F. Navarro, C. S. Frenk, and S. D. White, "The Structure of cold dark matter halos," *Astrophys. J.*, vol. 462, pp. 563–575, 1996. arXiv: astro-ph/9508025.

[107] J. F. Navarro, C. S. Frenk, and S. D. White, "A Universal density profile from hierarchical clustering," *Astrophys. J.*, vol. 490, pp. 493–508, 1997. arXiv: astro-ph/9611107.

[108] J. Dubinski and R. Carlberg, "The Structure of cold dark matter halos," *Astrophys. J.*, vol. 378, p. 496, 1991.

[109] J. Kormendy and L. C. Ho, "Coevolution (Or Not) of Supermassive Black Holes and Host Galaxies," *Ann. Rev. Astron. Astrophys.*, vol. 51, pp. 511–653, 2013. arXiv: 1304.7762 [astro-ph.CO].

[110] P. Gondolo and J. Silk, "Dark matter annihilation at the galactic center," *Phys. Rev. Lett.*, vol. 83, pp. 1719–1722, 1999. arXiv: astro-ph/9906391.

[111] S. Gillessen, F. Eisenhauer, S. Trippe, T. Alexander, R. Genzel, F. Martins, and T. Ott, "Monitoring stellar orbits around the Massive Black Hole in the Galactic Center," *Astrophys. J.*, vol. 692, pp. 1075–1109, 2009. arXiv: 0810.4674 [astro-ph].

[112] A. Ghez *et al.*, "Measuring Distance and Properties of the Milky Way's Central Supermassive Black Hole with Stellar Orbits," *Astrophys. J.*, vol. 689, pp. 1044–1062, 2008. arXiv: 0808.2870 [astro-ph].

[113] D. Hooper and B. L. Dingus, "Limits on supersymmetric dark matter from EGRET observations of the galactic center region," *Phys. Rev. D*, vol. 70, p. 113 007, 2004. arXiv: astro-ph/0210617.

[114] R. Aloisio, P. Blasi, and A. V. Olinto, "Neutralino annihilation at the Galactic Center revisited," *JCAP*, vol. 0405, p. 007, 2004. arXiv: astro-ph/0402588 [astro-ph].

[115] B. D. Fields, S. L. Shapiro, and J. Shelton, "Galactic Center Gamma-Ray Excess from Dark Matter Annihilation: Is There A Black Hole Spike?" *Phys. Rev. Lett.*, vol. 113, p. 151 302, 2014. arXiv: 1406.4856 [astro-ph.HE].

[116] A. V. Belikov, E. Moulin, and J. Silk, "Study of the very high energy gamma-ray spectrum from the Galactic Center and future prospects," *Phys. Rev. D*, vol. 94, no. 10, p. 103 005, 2016. arXiv: 1610.10003 [astro-ph.HE].

[117] P. Sandick, K. Sinha, and T. Yamamoto, "Black Holes, Dark Matter Spikes, and Constraints on Simplified Models with t-Channel Mediators," *Phys. Rev.*, vol. D98, no. 3, p. 035 004, 2018. arXiv: 1701.00067 [hep-ph].

[118] B. T. Chiang, S. L. Shapiro, and J. Shelton, "Faint dark matter annihilation signals and the Milky Way?s supermassive black hole," *Phys. Rev.*, vol. D102, no. 2, p. 023 030, 2020. arXiv: 1912.09446 [hep-ph].

[119] T. Lacroix, C. Bœhm, and J. Silk, "Ruling out thermal dark matter with a black hole induced spiky profile in the M87 galaxy," *Phys. Rev. D*, vol. 92, no. 4, p. 043 510, 2015. arXiv: 1505.00785 [astro-ph.GA].

[120] T. Lacroix, M. Karami, A. E. Broderick, J. Silk, and C. Boehm, "Unique probe of dark matter in the core of M87 with the Event Horizon Telescope," *Phys. Rev. D*, vol. 96, no. 6, p. 063 008, 2017. arXiv: 1611.01961 [astro-ph.GA].

[121] M. Wanders, G. Bertone, M. Volonteri, and C. Weniger, "No WIMP Mini-Spikes in Dwarf Spheroidal Galaxies," *JCAP*, vol. 04, p. 004, 2015. arXiv: 1409.5797 [astro-ph.HE].

[122] P. Ullio, H. Zhao, and M. Kamionkowski, "A Dark matter spike at the galactic center?" *Phys. Rev. D*, vol. 64, p. 043 504, 2001. arXiv: astro-ph/0101481.

[123] D. Merritt, M. Milosavljevic, L. Verde, and R. Jimenez, "Dark matter spikes and annihilation radiation from the galactic center," *Phys. Rev. Lett.*, vol. 88, p. 191 301, 2002. arXiv: astro-ph/0201376.

[124] O. Y. Gnedin and J. R. Primack, "Dark Matter Profile in the Galactic Center," *Phys. Rev. Lett.*, vol. 93, p. 061 302, 2004. arXiv: astro-ph/0308385.

[125] D. Merritt, "Evolution of the dark matter distribution at the galactic center," *Phys. Rev. Lett.*, vol. 92, p. 201 304, 2004. arXiv: astro-ph/0311594.

[126] R. Dave, D. N. Spergel, P. J. Steinhardt, and B. D. Wandelt, "Halo properties in cosmological simulations of selfinteracting cold dark matter," *Astrophys. J.*, vol. 547, pp. 574–589, 2001. arXiv: astro-ph/0006218 [astro-ph].

[127] M. Vogelsberger, J. Zavala, and A. Loeb, "Subhaloes in Self-Interacting Galactic Dark Matter Haloes," *Mon. Not. Roy. Astron. Soc.*, vol. 423, p. 3740, 2012. arXiv: 1201.5892 [astro-ph.CO].

[128] A. H. G. Peter, M. Rocha, J. S. Bullock, and M. Kaplinghat, "Cosmological Simulations with Self-Interacting Dark Matter II: Halo Shapes vs. Observations," *Mon. Not. Roy. Astron. Soc.*, vol. 430, p. 105, 2013. arXiv: 1208.3026 [astro-ph.CO].

[129] J. Zavala, M. Vogelsberger, and M. G. Walker, "Constraining Self-Interacting Dark Matter with the Milky Way's dwarf spheroidals," *Mon. Not. Roy. Astron. Soc.*, vol. 431, pp. L20–L24, 2013. arXiv: 1211.6426 [astro-ph.CO].

[130] M. Vogelsberger, J. Zavala, F.-Y. Cyr-Racine, C. Pfrommer, T. Bringmann, and K. Sigurdson, "ETHOS – an effective theory of structure formation: dark matter physics as a possible explanation of the small-scale CDM problems," *Mon. Not. Roy. Astron. Soc.*, vol. 460, no. 2, pp. 1399–1416, 2016. arXiv: 1512.05349 [astro-ph.CO].

[131] M. S. Fischer, M. Brüggen, K. Schmidt-Hoberg, K. Dolag, F. Kahlhoefer, A. Ragagnin, and A. Robertson, "N-body simulations of dark matter with frequent self-interactions," Dec. 2020. arXiv: 2012.10277 [astro-ph.CO].

[132] P. Creasey, O. Sameie, L. V. Sales, H.-B. Yu, M. Vogelsberger, and J. Zavala, "Spreading out and staying sharp ? creating diverse rotation curves via baryonic and self-interaction effects," *Mon. Not. Roy. Astron. Soc.*, vol. 468, no. 2, pp. 2283–2295, 2017. arXiv: 1612.03903 [astro-ph.GA].

[133] T. Ren, A. Kwa, M. Kaplinghat, and H.-B. Yu, "Reconciling the Diversity and Uniformity of Galactic Rotation Curves with Self-Interacting Dark Matter," *Phys. Rev.*, vol. X9, no. 3, p. 031 020, 2019. arXiv: 1808.05695 [astro-ph.GA].

[134] M. Kaplinghat, M. Valli, and H.-B. Yu, "Too Big To Fail in Light of Gaia," *Mon. Not. Roy. Astron. Soc.*, vol. 490, no. 1, pp. 231–242, 2019. arXiv: 1904.04939 [astro-ph.GA].

[135] O. Sameie, H.-B. Yu, L. V. Sales, M. Vogelsberger, and J. Zavala, "Self-Interacting Dark Matter Subhalos in the Milky Way's Tides," *Phys. Rev. Lett.*, vol. 124, no. 14, p. 141 102, 2020. arXiv: 1904.07872 [astro-ph.GA].

[136] F. Kahlhoefer, M. Kaplinghat, T. R. Slatyer, and C.-L. Wu, "Diversity in density profiles of self-interacting dark matter satellite halos," *JCAP*, vol. 1912, p. 010, 2019. arXiv: 1904.10539 [astro-ph.GA].

[137] D. Yang, H.-B. Yu, and H. An, "Self-Interacting Dark Matter and the Origin of Ultradiffuse Galaxies NGC1052-DF2 and -DF4," *Phys. Rev. Lett.*, vol. 125, no. 11, p. 111 105, 2020. arXiv: 2002.02102 [astro-ph.GA].

[138] L. Sagunski, S. Gad-Nasr, B. Colquhoun, A. Robertson, and S. Tulin, "Velocity-dependent Self-interacting Dark Matter from Groups and Clusters of Galaxies," Jun. 2020. arXiv: 2006.12515 [astro-ph.CO].

[139] K. E. Andrade, J. Fuson, S. Gad-Nasr, D. Kong, Q. Minor, M. G. Roberts, and M. Kaplinghat, "A Stringent Upper Limit on Dark Matter Self-Interaction Cross Section from Cluster Strong Lensing," Dec. 2020. arXiv: 2012.06611 [astro-ph.CO].

[140] S. L. Shapiro and V. Paschalidis, "Self-interacting dark matter cusps around massive black holes," *Phys. Rev. D*, vol. 89, no. 2, p. 023 506, 2014. arXiv: 1402.0005 [astro-ph.CO].

[141] S. Tremaine *et al.*, "The slope of the black hole mass versus velocity dispersion correlation," *Astrophys. J.*, vol. 574, pp. 740–753, 2002. arXiv: astro-ph/0203468.

[142] S. L. Shapiro and A. P. Lightman, "The distribution of stars around a massive black hole," *Nature.*, vol. 262, no. 5571, pp. 743–745, 1976.

[143] R. Huo, M. Kaplinghat, Z. Pan, and H.-B. Yu, "Signatures of Self-Interacting Dark Matter in the Matter Power Spectrum and the CMB," *Phys. Lett. B*, vol. 783, pp. 76–81, 2018. arXiv: 1709.09717 [hep-ph].

[144] E. Vasiliev, "Dark matter annihilation near a black hole: Plateau vs. weak cusp," *Phys. Rev. D*, vol. 76, p. 103 532, 2007. arXiv: 0707.3334 [astro-ph].

[145] S. L. Shapiro and J. Shelton, "Weak annihilation cusp inside the dark matter spike about a black hole," *Phys. Rev. D*, vol. 93, no. 12, p. 123 510, 2016. arXiv: 1606.01248 [astro-ph.HE].

[146] M. Kaplinghat, R. E. Keeley, T. Linden, and H.-B. Yu, "Tying Dark Matter to Baryons with Self-interactions," *Phys. Rev. Lett.*, vol. 113, p. 021 302, 2014. arXiv: 1311.6524 [astro-ph.CO].

[147] A. Robertson *et al.*, "The diverse density profiles of galaxy clusters with self-interacting dark matter plus baryons," *Mon. Not. Roy. Astron. Soc.*, vol. 476, no. 1, pp. L20–L24, 2018. arXiv: 1711.09096 [astro-ph.CO].

[148] A. Robertson, R. Massey, V. Eke, J. Schaye, and T. Theuns, "The surprising accuracy of isothermal Jeans modelling of self-interacting dark matter density profiles," Sep. 2020. arXiv: 2009.07844 [astro-ph.CO].

[149] D. Merritt, "Single and binary black holes and their influence on nuclear structure," in *Carnegie Observatories Centennial Symposium. 1. Coevolution of Black Holes and Galaxies*, Jan. 2003. arXiv: astro-ph/0301257.

[150] M. Cirelli, G. Corcella, A. Hektor, G. Hutsi, M. Kadastik, P. Panci, M. Raidal, F. Sala, and A. Strumia, "PPPC 4 DM ID: A Poor Particle Physicist Cookbook for Dark Matter Indirect Detection," *JCAP*, vol. 03, p. 051, 2011, [Erratum: JCAP 10, E01 (2012)]. arXiv: 1012.4515 [hep-ph].

[151] S. Amoroso, S. Caron, A. Jueid, R. Ruiz de Austri, and P. Skands, "Estimating QCD uncertainties in Monte Carlo event generators for gamma-ray dark matter searches," *JCAP*, vol. 05, p. 007, 2019. arXiv: 1812.07424 [hep-ph].

[152] M. Kaplinghat, T. Linden, and H.-B. Yu, "Galactic Center Excess in γ Rays from Annihilation of Self-Interacting Dark Matter," *Phys. Rev. Lett.*, vol. 114, no. 21, p. 211 303, 2015. arXiv: 1501.03507 [hep-ph].

[153] T. Bringmann, F. Kahlhoefer, K. Schmidt-Hoberg, and P. Walia, "Strong constraints on self-interacting dark matter with light mediators," *Phys. Rev. Lett.*, vol. 118, no. 14, p. 141 802, 2017. arXiv: 1612.00845 [hep-ph].

[154] M. Cirelli, P. Panci, K. Petraki, F. Sala, and M. Taoso, "Dark Matter's secret liaisons: phenomenology of a dark U(1) sector with bound states," *JCAP*, vol. 05, p. 036, 2017. arXiv: 1612.07295 [hep-ph].

[155] X. Chu, C. Garcia-Cely, and T. Hambye, "Can the relic density of self-interacting dark matter be due to annihilations into Standard Model particles?" *JHEP*, vol. 11, p. 048, 2016. arXiv: 1609.00399 [hep-ph].

[156] A. Kamada, M. Yamada, and T. T. Yanagida, "Self-interacting dark matter with a vector mediator: kinetic mixing with the $\mathrm{U}(1)_{(B-L)_3}$ gauge boson," *JHEP*, vol. 03, p. 021, 2019. arXiv: 1811.02567 [hep-ph].

[157] X. Chu, C. Garcia-Cely, and H. Murayama, "Velocity Dependence from Resonant Self-Interacting Dark Matter," *Phys. Rev. Lett.*, vol. 122, no. 7, p. 071 103, 2019. arXiv: 1810.04709 [hep-ph].

[158] N. Bernal, X. Chu, S. Kulkarni, and J. Pradler, "Self-interacting dark matter without prejudice," *Phys. Rev. D*, vol. 101, no. 5, p. 055 044, 2020. arXiv: 1912.06681 [hep-ph].

[159] Y.-J. Kang and H. M. Lee, "Dark matter self-interactions from spin-2 mediators," Feb. 2020. arXiv: 2002.12779 [hep-ph].

[160] M. Valli and H.-B. Yu, "Dark matter self-interactions from the internal dynamics of dwarf spheroidals," *Nat. Astron.*, vol. 2, pp. 907–912, 2018. arXiv: 1711.03502 [astro-ph.GA].

[161] J. I. Read, M. G. Walker, and P. Steger, "The case for a cold dark matter cusp in Draco," *Mon. Not. Roy. Astron. Soc.*, vol. 481, no. 1, pp. 860–877, 2018. arXiv: 1805.06934 [astro-ph.GA].

[162] H. Nishikawa, K. K. Boddy, and M. Kaplinghat, "Accelerated core collapse in tidally stripped self-interacting dark matter halos," *Phys. Rev. D*, vol. 101, no. 6, p. 063 009, 2020. arXiv: 1901.00499 [astro-ph.GA].

[163] C. A. Correa, "Constraining Velocity-dependent Self-Interacting Dark Matter with the Milky Way's dwarf spheroidal galaxies," Jul. 2020. arXiv: 2007.02958 [astro-ph.GA].

[164] H. C. Turner, M. R. Lovell, J. Zavala, and M. Vogelsberger, "The Onset of Gravothermal Core Collapse in Velocity Dependent Self-Interacting Dark Matter Subhaloes," Oct. 2020. arXiv: 2010.02924 [astro-ph.GA].

[165] K. N. Abazajian, S. Horiuchi, M. Kaplinghat, R. E. Keeley, and O. Macias, "Strong constraints on thermal relic dark matter from Fermi-LAT observations of

the Galactic Center," *Phys. Rev. D*, vol. 102, no. 4, p. 043 012, 2020. arXiv: 2003.10416 [hep-ph].

[166] O. Sameie, P. Creasey, H.-B. Yu, L. V. Sales, M. Vogelsberger, and J. Zavala, "The impact of baryonic discs on the shapes and profiles of self-interacting dark matter haloes," *Mon. Not. Roy. Astron. Soc.*, vol. 479, no. 1, pp. 359–367, 2018. arXiv: 1801.09682 [astro-ph.GA].

[167] K. Gebhardt and J. Thomas, "The Black Hole Mass, Stellar M/L, and Dark Halo in M87," *Astrophys. J.*, vol. 700, pp. 1690–1701, 2009. arXiv: 0906.1492 [astro-ph.CO].

[168] K. Akiyama *et al.*, "First M87 Event Horizon Telescope Results. VI. The Shadow and Mass of the Central Black Hole," *Astrophys. J. Lett.*, vol. 875, no. 1, p. L6, 2019. arXiv: 1906.11243 [astro-ph.GA].

[169] S. S. Doeleman *et al.*, "Jet Launching Structure Resolved Near the Supermassive Black Hole in M87," *Science*, vol. 338, p. 355, 2012. arXiv: 1210.6132 [astro-ph.HE].

[170] K. Akiyama *et al.*, "230 GHz VLBI observations of M87: event-horizon-scale structure during an enhanced very-high-energy γ-ray state in 2012," *Astrophys. J.*, vol. 807, no. 2, p. 150, 2015. arXiv: 1505.03545 [astro-ph.HE].

[171] S. Balberg and S. L. Shapiro, "Gravothermal collapse of selfinteracting dark matter halos and the origin of massive black holes," *Phys. Rev. Lett.*, vol. 88, p. 101 301, 2002. arXiv: astro-ph/0111176 [astro-ph].

[172] W.-X. Feng, H.-B. Yu, and Y.-M. Zhong, "Seeding Supermassive Black Holes with Self-Interacting Dark Matter," Oct. 2020. arXiv: 2010.15132 [astro-ph.CO].

[173] D. Tucker-Smith and N. Weiner, "Inelastic dark matter," *Phys. Rev. D*, vol. 64, p. 043 502, 2001. arXiv: hep-ph/0101138.

[174] R. Bernabei *et al.*, "First results from DAMA/LIBRA and the combined results with DAMA/NaI," *Eur. Phys. J. C*, vol. 56, pp. 333–355, 2008. arXiv: 0804.2741 [astro-ph].

[175] A. Berlin and F. Kling, "Inelastic Dark Matter at the LHC Lifetime Frontier: ATLAS, CMS, LHCb, CODEX-b, FASER, and MATHUSLA," *Phys. Rev. D*, vol. 99, no. 1, p. 015 021, 2019. arXiv: 1810.01879 [hep-ph].

[176] R. Nan, D. Li, C. Jin, Q. Wang, L. Zhu, W. Zhu, H. Zhang, Y. Yue, and L. Qian, "The Five-Hundred-Meter Aperture Spherical Radio Telescope (FAST) Project," *Int. J. Mod. Phys. D*, vol. 20, pp. 989–1024, 2011. arXiv: 1105.3794 [astro-ph.IM].

[177] C. Ng, "Pulsar science with the CHIME telescope," *IAU Symp.*, vol. 337, S. Sanidas, P. Weltevrede, L. L. Preston, and B. B. P. Perera, Eds., pp. 179–182, 2017. arXiv: 1711.02104 [astro-ph.IM].

[178] C. L. Carilli and S. Rawlings, "Science with the Square Kilometer Array: Motivation, key science projects, standards and assumptions," *New Astron. Rev.*, vol. 48, p. 979, 2004. arXiv: astro-ph/0409274.

[179] J. P. Gardner *et al.*, "The James Webb Space Telescope," *Space Sci. Rev.*, vol. 123, p. 485, 2006. arXiv: astro-ph/0606175.

[180] W. Skidmore *et al.*, "Thirty Meter Telescope Detailed Science Case: 2015," *Res. Astron. Astrophys.*, vol. 15, no. 12, pp. 1945–2140, 2015. arXiv: 1505.01195 [astro-ph.IM].

[181] T. Andersen, A. Ardeberg, J. Beckers, A. Goncharov, M. Owner-Petersen, H. Riewaldt, R. Snel, and D. Walker, "The euro50 extremely large telescope," in *Future Giant Telescopes*, ser. The International Society for Optical Engineering, vol. 4840, 2003, pp. 214–225.

[182] M. Baryakhtar, J. Bramante, S. W. Li, T. Linden, and N. Raj, "Dark Kinetic Heating of Neutron Stars and An Infrared Window On WIMPs, SIMPs, and Pure Higgsinos," *Phys. Rev. Lett.*, vol. 119, no. 13, p. 131 801, 2017. arXiv: 1704.01577 [hep-ph].

[183] N. Raj, P. Tanedo, and H.-B. Yu, "Neutron stars at the dark matter direct detection frontier," *Phys. Rev. D*, vol. 97, no. 4, p. 043 006, 2018. arXiv: 1707.09442 [hep-ph].

[184] N. F. Bell, G. Busoni, and S. Robles, "Heating up Neutron Stars with Inelastic Dark Matter," *JCAP*, vol. 09, p. 018, 2018. arXiv: 1807.02840 [hep-ph].

[185] A. Joglekar, N. Raj, P. Tanedo, and H.-B. Yu, "Dark kinetic heating of neutron stars from contact interactions with relativistic targets," *Phys. Rev. D*, vol. 102, no. 12, p. 123 002, 2020. arXiv: 2004.09539 [hep-ph].

[186] A. Joglekar, N. Raj, P. Tanedo, and H.-B. Yu, "Relativistic capture of dark matter by electrons in neutron stars," *Phys. Lett.*, vol. B, p. 135 767, 2020. arXiv: 1911.13293 [hep-ph].

[187] J. Bramante and N. Song, "Electric But Not Eclectic: Thermal Relic Dark Matter for the XENON1T Excess," *Phys. Rev. Lett.*, vol. 125, no. 16, p. 161 805, 2020. arXiv: 2006.14089 [hep-ph].

[188] M. Dutta, S. Mahapatra, D. Borah, and N. Sahu, "Self-interacting Inelastic Dark Matter in the light of XENON1T excess," *Phys. Rev. D*, vol. 103, no. 9, p. 095 018, 2021. arXiv: 2101.06472 [hep-ph].

[189] J. P. Lees *et al.*, "Search for a Dark Photon in e^+e^- Collisions at BaBar," *Phys. Rev. Lett.*, vol. 113, no. 20, p. 201 801, 2014. arXiv: 1406.2980 [hep-ex].

[190] P. deNiverville, M. Pospelov, and A. Ritz, "Observing a light dark matter beam with neutrino experiments," *Phys. Rev. D*, vol. 84, p. 075 020, 2011. arXiv: 1107.4580 [hep-ph].

[191] M. Duch and B. Grzadkowski, "Resonance enhancement of dark matter interactions: the case for early kinetic decoupling and velocity dependent resonance width," *JHEP*, vol. 09, p. 159, 2017. arXiv: 1705.10777 [hep-ph].

[192] J. Yang *et al.*, "Constraining self-interacting dark matter with the full dataset of PandaX-II," *Sci. China Phys. Mech. Astron.*, vol. 64, no. 11, p. 111 062, 2021. arXiv: 2104.14724 [hep-ex].

[193] J. Bramante, P. J. Fox, G. D. Kribs, and A. Martin, "Inelastic frontier: Discovering dark matter at high recoil energy," *Phys. Rev. D*, vol. 94, no. 11, p. 115 026, 2016. arXiv: 1608.02662 [hep-ph].

[194] T. Lin, "Dark matter models and direct detection," *PoS*, vol. 333, p. 009, 2019. arXiv: 1904.07915 [hep-ph].

[195] J. M. Pearson, N. Chamel, A. Y. Potekhin, A. F. Fantina, C. Ducoin, A. K. Dutta, and S. Goriely, "Unified equations of state for cold non-accreting neutron stars with Brussels–Montreal functionals – I. Role of symmetry energy," *Mon. Not. Roy. Astron. Soc.*, vol. 481, no. 3, pp. 2994–3026, 2018, [Erratum: Mon.Not.Roy.Astron.Soc. 486, 768 (2019)]. arXiv: 1903.04981 [astro-ph.HE].

[196] N. F. Bell, G. Busoni, and S. Robles, "Capture of Leptophilic Dark Matter in Neutron Stars," *JCAP*, vol. 06, p. 054, 2019. arXiv: 1904.09803 [hep-ph].

[197] R. Garani, Y. Genolini, and T. Hambye, "New Analysis of Neutron Star Constraints on Asymmetric Dark Matter," *JCAP*, vol. 05, p. 035, 2019. arXiv: 1812.08773 [hep-ph].

[198] F. Anzuini, N. F. Bell, G. Busoni, T. F. Motta, S. Robles, A. W. Thomas, and M. Virgato, "Improved treatment of dark matter capture in neutron stars III: nucleon and exotic targets," *JCAP*, vol. 11, no. 11, p. 056, 2021. arXiv: 2108.02525 [hep-ph].

[199] Y. Cui, "A Review of WIMP Baryogenesis Mechanisms," *Mod. Phys. Lett. A*, vol. 30, no. 37, p. 1 530 028, 2015. arXiv: 1510.04298 [hep-ph].

[200] S. Mandal, N. Rojas, R. Srivastava, and J. W. F. Valle, "Dark matter as the origin of neutrino mass in the inverse seesaw mechanism," *Phys. Lett. B*, vol. 821, p. 136 609, 2021. arXiv: 1907.07728 [hep-ph].

[201] C. Alvarado, C. Bonilla, J. Leite, and J. W. F. Valle, "Phenomenology of fermion dark matter as neutrino mass mediator with gauged B-L," *Phys. Lett. B*, vol. 817, p. 136 292, 2021. arXiv: 2102.07216 [hep-ph].

[202] F. Wilczek, "Problem of Strong P and T Invariance in the Presence of Instantons," *Phys. Rev. Lett.*, vol. 40, pp. 279–282, 1978.

[203] L. Di Luzio, M. Giannotti, E. Nardi, and L. Visinelli, "The landscape of QCD axion models," *Phys. Rept.*, vol. 870, pp. 1–117, 2020. arXiv: 2003.01100 [hep-ph].

[204] L. Vietze, P. Klos, J. Menéndez, W. C. Haxton, and A. Schwenk, "Nuclear structure aspects of spin-independent WIMP scattering off xenon," *Phys. Rev. D*, vol. 91, no. 4, p. 043 520, 2015. arXiv: 1412.6091 [nucl-th].

[205] E. Aprile *et al.*, "Dark Matter Search Results from a One Ton-Year Exposure of XENON1T," *Phys. Rev. Lett.*, vol. 121, no. 11, p. 111 302, 2018. arXiv: 1805.12562 [astro-ph.CO].